

Chapter 2

Background

Lasse Løvstakken

Dept. Circulation and Medical Imaging, NTNU

The following chapter contains information that is included to give the unfamiliar reader a short introduction to diagnostic ultrasound imaging and conventional methods and terms used in this context. It also includes more in-depth information about the concept of color flow imaging (CFI), the modality under investigation in this thesis work. An overview of conventional methods is given, and current challenges and limitations are reviewed. A review is finally given on previous work in the two main topics of the thesis work, that of two-dimensional velocity estimation and adaptive clutter filtering in CFI.

2.1 Diagnostic ultrasound imaging

2.1.1 Background

The history of diagnostic ultrasound traces back to the 1940s, when the concept of using ultrasound to image the human interior was conceived based on knowledge of pulse-echo imaging from SONAR and technology from ultrasonic metal flaw detectors available at the time. This emerging technology matured during the forties, and by the end of the decade systematic research into its diagnostic use began in several research groups over the world. Some of the first descriptions of diagnostic ultrasound imaging was reported in the early fifties through the pioneering work of Wild and Reid, Howry and Bliss, and Edler and Hertz [1–3]. An important foundation for the use of this technology in medicine was the discovery of new piezoelectric materials in the mid-forties, which allowed for the generation of short high frequency pulses in the MHz range.

As a diagnostic tool, ultrasound was first conceived as a tool for tissue characterization, i.e. with the ability to differentiate between different types of tissue such as cancerous and normal tissue. Although research in this area is still ongoing, this goal has arguably still not been reached today [4, 5]. Demonstrations of ultrasound imaging equipment were presented in the fifties. However, it was not until the advent of transistor technology that equipment could be made that would allow for mainstream use. The first commercial B-mode (brightness mode) instruments became available in

the early sixties, offering static images of the human interior based on the received signal envelope. Further advances in transistor technology lead to the first real-time B-mode scanners in the late sixties and through the seventies [6–8].

From the late fifties, effort was also put into registering movement with ultrasound through the Doppler shift of the received signal. The first effort is usually attributed to Satumora in 1957 [9]. The first commercial Doppler instruments appeared in the sixties based on the continuous wave (CW) approach, which did not include any depth information. Pulsed wave (PW) Doppler instruments for measuring blood flow velocity at specific depths was described in the late sixties [10–12]. The development of the scan converter further allowed for duplex operation of both Doppler and B-mode imaging in the late seventies, while real-time two-dimensional Doppler mapping became feasible in the mid-eighties. A formidable development has taken place due to dedicated research in both the technical and clinical community [13, 14].

Ultrasound imaging is today used in a wide range of clinical contexts. Perhaps the most well known application is that in obstetrics and fetal medicine [15], where ultrasound examinations are used to investigate the health of the fetus during pregnancies. Clinical research in this area has been extensive since the late sixties, and ultrasound examinations can today reveal many potential health risks, reducing the morbidity and mortality of newborns. Due to its high imaging frame rate, ultrasound has also found particular use in the diagnosis of cardiovascular disease, where the dynamics of the heart muscle and the blood flow in the heart and arteries are important measures. The development of Doppler ultrasound for measuring blood flow and tissue velocities, has provided physicians with a valuable tool for diagnosis in the cardiovascular system [16, 17]. Ultrasound imaging is further used in many other areas of medicine, such as the screening for breast cancer in women, detection of abnormalities and cancer in the internal organs. It is also used intraoperatively in for instance heart- and neurosurgery as a tool for quality control. For a more complete description of ultrasound imaging techniques and applications in medicine, please refer to one of the many textbooks available, such as [18–21].

In the following subsections, a brief look at the basic principles of ultrasound imaging, and at the design of modern ultrasound imaging systems will be given.

2.1.2 Basic principles of ultrasound imaging

Ultrasound is defined as pressure waves with frequencies above the human audible range of 20 kHz. Pressure waves propagate through a medium. In diagnostic ultrasound imaging, longitudinal pressure wave pulses with center frequencies in the range of 2-15 MHz are transmitted into the human tissue. As the pressure wave propagate, it interacts with different tissue characteristics through scattering and attenuation processes. This fundamental mechanism is the foundation of ultrasound imaging. The pressure amplitude of the backscattered ultrasound can be registered and used to form an image of the different tissue media present.

The properties of a tissue medium can be described by a given density ρ and compressibility κ . It is the local differences in density and compressibility that causes the scattering of ultrasound. The basic equation governing pressure wave propagation

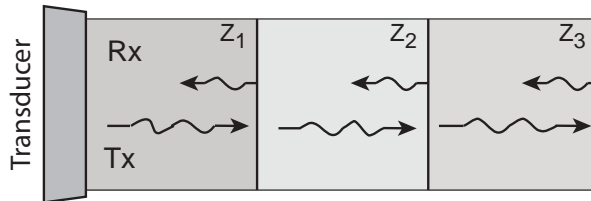


Figure 2.1: The concept of pulse-echo ultrasound imaging. An ultrasound pulse is emitted into the tissue, and is scattered at interfaces between different types of tissue Z_1 , Z_2 , and Z_3 . The backscattered signal is received by the same transducer and form the basis for the ultrasound image.

can be derived by considering the conservation of mass and momentum. Assuming a homogenous medium, and linear propagation where the displacement of scattering volumes is linearly proportional to the change in pressure, the basic equation governing the propagation of a pressure wave $p(\mathbf{r}, t)$ is given by [22]

$$\nabla^2 p(\mathbf{r}, t) - \frac{1}{c^2} \frac{\partial^2 p(\mathbf{r}, t)}{\partial t^2} = 0, \quad (2.1)$$

where \mathbf{r} is a spatial position vector, t is time, and $c = \frac{1}{\sqrt{\rho\kappa}}$ is the speed of sound in the medium. The speed of sound in human tissue has been measured to be 1540 m/s on average, with only a small range for different types of soft tissue [23]. The assumption of a constant value for the speed of sound is fundamental in conventional ultrasound imaging, and allows for a simple conversion between imaging depth and receive time in pulse-echo operation.

The ultrasonic waves are attenuated as they travel through the tissue due to power absorptions, scattering losses, and the geometric spreading of the ultrasound beam [22]. This attenuation limit the penetration depth in ultrasound imaging. Because the spatial resolution of an ultrasound image is proportional to the frequency of the transmitted pulse, one would in principle use higher frequencies. Unfortunately the attenuation of ultrasonic waves is frequency dependent, and the optimal working frequency is a compromise between resolution and penetration. The attenuation in human soft tissue is usually approximated to be 0.5 dB/cmMHz one way [24].

Conventional ultrasound imaging is pulse-echo imaging, a concept illustrated in Fig. 2.7. An ultrasound transducer transfers pressure waves into the tissue, and also receives the backscattered signal produced as the wave encounters differences in tissue properties across its path. The backscattered signal is a measure of the different tissue properties and can be used to form an image. Scattering objects can be divided into three basic types. An object large compared to the wavelength of the transmitted pulse will reflect the ultrasound wave in a specular way. Scattering objects comparable to the wavelength will scatter the ultrasound wave directionally. Finally, scattering objects small compared to the wavelength will scatter the incoming ultrasound wave in an omnidirectional way, so-called Rayleigh scattering. As an example, specular

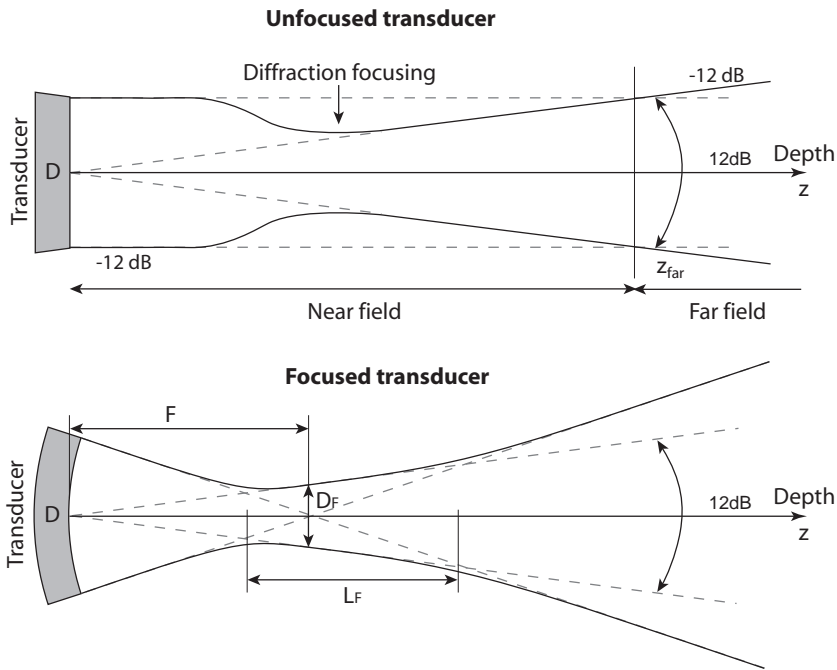


Figure 2.2: The beam profile of a plane unfocused (upper) and focused transducer (lower). The course of the unfocused beam can be divided into a near field and far field region. In the near field diffraction effects are prominent and cause a convergence of the beam known as diffraction focusing. By focusing, a narrow beam width can be achieved in the near field over a limited depth region.

reflectors could be structures such as bone or vessel walls, while Rayleigh scattering results when the ultrasound beam encounters the small red blood cells. Combinations of these scattering processes are typically present throughout an ultrasound image.

Beam formation

When the wavelength of the transmitted pressure wave becomes small compared to the transmitting aperture, the sound beam generated will become directional. This is the case for the unfocused ultrasound beam illustrated in the upper schematic of Fig. 2.2. It is useful to divide the course of the sound beam into specific regions in depth, the near and far field. In the near field diffraction effects are prominent. These effects are present due to the limited aperture used, and will cause the beam to converge, a phenomenon called diffraction focusing. The extreme near field is often defined as the region where the beam is a close replica in width to that of the aperture used. The far field is defined as the region where the pressure wave amplitude fall off at a fixed rate. The transition between the near and far field is for a plane circular transducer

given by

$$z_{far} = \frac{D^2}{2\lambda}, \quad (2.2)$$

where D is the diameter of the aperture, and λ is the wavelength of the emitted pulse. The one way beam width is usually defined as the -12 dB drop in signal power. As an example, consider a transducer with an aperture diameter of 2 cm and a center frequency of 2.5 MHz. The start of the far field region is then given by

$$z_{far} = \frac{0.02^2 \cdot 2.5e6}{2 \cdot 1540} \text{ cm} = 32 \text{ cm} \quad (2.3)$$

In other words, ultrasound image formation is made in the near field of the transducer.

The beam can be focused by curving the aperture, by using a lens, or by using transducer arrays and electronic delays between the different array elements. When focusing the far field is effectively brought into the near field, and a narrow beam width can then be achieved at a specific depth in a limited region. In order to achieve efficient focusing, the focus point must lie in the near field of the beam as defined for a circular transducer in (2.2). A focused beam profile is shown in the lower schematic of Fig. 2.2. The beam width D_F determines the lateral resolution of the imaging system, and is for a focused transducer given by (-3 dB beam width)

$$D_F = \frac{\lambda}{D} F = F_{\#} \lambda, \quad (2.4)$$

where F is the distance to the focus point, D is the aperture diameter, λ is the wavelength. $F_{\#}$ is the focus distance measured in apertures, the F-number of the imaging system. The focal depth L_F of the beam defines the effective depth region of uniform beam width as given at the focus depth. The (-1 dB) focal depth is given by

$$L_F = 4 \cdot \lambda F_{\#}^2. \quad (2.5)$$

For a transducer aperture of 2 cm with a center frequency emission of 2.5 MHz, focused at 7 cm, the beam width and focus depth is equal to

$$D_F = \frac{0.07 \cdot 1540}{0.02 \cdot 2.5e6} \text{ cm} = 0.22 \text{ cm}, \quad L_F = 4 \cdot \frac{0.07^2 \cdot 1540}{0.02^2 \cdot 2.5e6} \text{ cm} = 3.0 \text{ cm} \quad (2.6)$$

The F-number defines the lateral resolution in focus as given by (2.4), and is therefore desired to be low to achieve a narrow beam width. However as seen in (2.5), the depth of focus is proportional to the F-number squared. Using too low F-numbers may therefore concentrate the sound energy in a small region along the beam axis, and the appropriate F-number must therefore be optimized according to a given transducer design and application.

The beam shape can be further optimized using *apodization*, *dynamic aperture*, and *dynamic focus*. The concept of apodization is to weight the individual elements according to a window function. This will reduce the beam side lobe level at the expense of a broader main lobe. Dynamic aperture is further used to create a more uniform beam width in depth, by reducing the aperture size used at closer depths on receive to keep the F-number as constant as possible. The concept of dynamic focus is to sweep the focus electronically on receive according to depth.

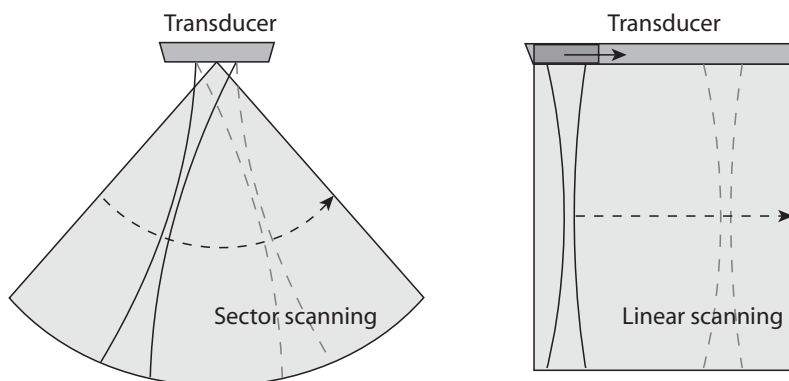


Figure 2.3: Two common ultrasound scanning modes, the sector and linear scan.

Image formation

Image formation is done by sweeping the ultrasound beam over a region of interest, and registering the backscattered signal in each direction. The sweeping of the beam is today typically done electronically using transducer arrays, but is also still done mechanically in certain applications, for instance in high frequency imaging systems. Sweeping the beam electronically can be done in different ways. Two standard techniques are depicted in Fig. 2.3. The sector scan uses transmission delays on the array elements to not only focus the beam, but also to steer the beam in a desired direction. This is called phased array imaging, and is most widely used in cardiac applications where the acoustic window between the ribs is limited. To be able to steer the beam at larger angles, the array elements must be small compared to the wavelength in order to achieve efficient focusing and to avoid grating lobes. Grating lobes are repetitions of the main lobe in space due to the division of the aperture into elements. A common design criteria is to require an element size of $a = \lambda/2$, which in theory allows for efficient steering in a sector of 90 degrees without grating lobes.

Another type of sweeping is the linear scan. A larger aperture is typically used, with larger elements of size $\sim 1.5\lambda$ as steering requirements are limited. A smaller subaperture is used to form a beam at a given offset from the center of the transducer. This subaperture is swept over the aperture to produce a rectangular image region. Linear scans are used in vascular and abdominal applications. In abdominal applications it is also common to curve the transducer aperture to achieve a broader field of view and a better contact with the abdomen, so-called curvilinear arrays.

Display modes

Several different display modes have been introduced since the beginning of ultrasound imaging. The most basic display modality today is the B-mode modality, which shows a two-dimensional image of tissue in gray scale. Images are made based on the

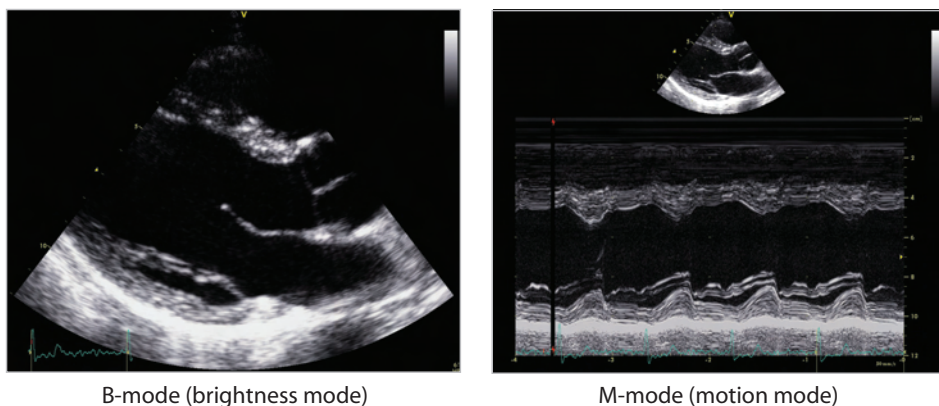


Figure 2.4: The B-mode and M-mode imaging of a healthy human heart.

received signal envelope. Due to the high dynamic range of the received signal from different tissue structures, the signal is logarithmically compressed before display to show both weak and strong echoes simultaneously. In B-mode, a high spatial resolution is important in order to resolve close targets. A high frame rate is also desired in many clinical applications to investigate the dynamics of structures.

Another common modality is the M-mode (motion mode), which displays the envelope of the acquired signal along a specific beam direction over time. This one-dimensional modality has a very high imaging frame rate and is suitable for investigating rapid movements of tissue structures, for instance the movement of the heart valves. M-mode images along curved lines, called curved M-mode, is also used based on two-dimensional acquisitions. In Fig. 2.4, a standard B-mode and M-mode image of a healthy human heart is shown.

In addition to the two major tissue imaging modalities described, a number of Doppler related modalities have been introduced. Continuous wave (CW) and pulsed wave (PW) spectral Doppler is used to investigate the blood flow distribution in the heart and arteries. Two-dimensional Doppler mapping, or color flow imaging (CFI), became a standard modality in the early nineties, and shows the distribution of flow velocities in a region of interest. Duplex operation of both B-mode and spectral Doppler or CFI, and triplex modalities of all three is also available on modern systems.

Static and electrocardiogram-gated 3-D images have been available for some time for abdominal imaging using mechanically steered transducers. In recent years, dynamic three-dimensional imaging has also become available. Using 2-D array technology, real-time 3-D images of the heart anatomy and blood flow can be obtained. The new information available can for instance be beneficial in the diagnosis of the heart valve disease.

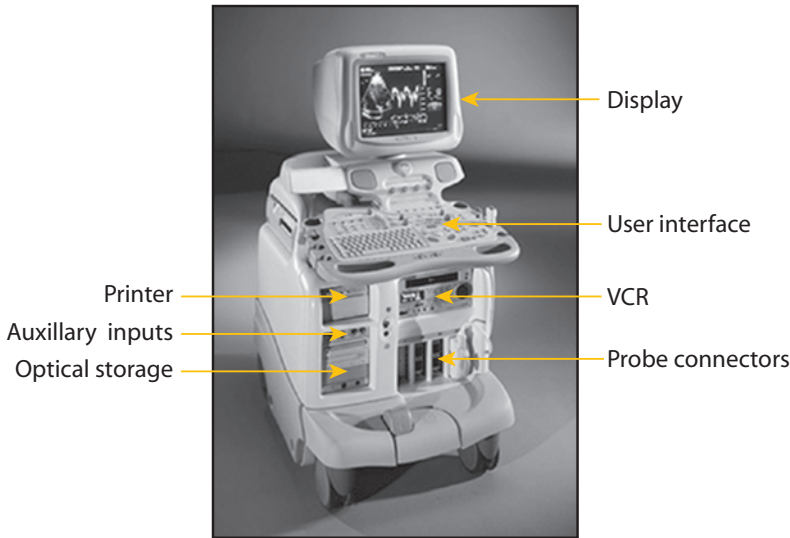


Figure 2.5: The GE Vivid 7 ultrasound system. Different parts of the system has been labeled.

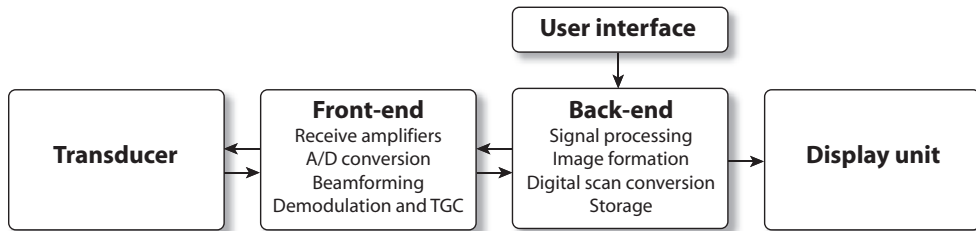


Figure 2.6: Block diagram of modern generic ultrasound system.

2.1.3 Building blocks of an ultrasound imaging system

A modern high-end scanner is shown in Fig. 2.5. These systems contain a user interface and display, probe connectors, an optical storage unit, ECG and other auxiliary input connectors, a thermal printer, and often units for supporting old recordings such as a VCR. Modern systems are designed to be portable within hospital buildings, but laptop size systems are now also available which includes most of the functionality of high-end scanners. The basic building blocks and signal chain of a modern ultrasound imaging system is shown in Fig. 2.6, and will be described in the following subsections.

Transducer

The transducer is an indispensable part of the ultrasound imaging system, responsible for the transmission and reception of ultrasonic pressure waves. A typical transducer today consists of an array of piezoelectric elements. On transmission, these piezoelectric elements vibrate in response to an external electric field, creating ultrasonic waves. On receive, the piezoelectric elements vibrate in response to an external pressure, producing an electrical signal. Ultrasound pulse emission timing and array element apodization can be controlled electronically, and allows for flexible beam shaping and electronic focusing and steering of the beam. Transducers come in different shapes and sizes designed for specific clinical applications. Also, due to the limited frequency bandwidth of the currently available piezoelectric ceramic materials, transducers also have to be designed to work in a specific frequency range, based on the demands of penetration in a given clinical application. For instance, a transducer designed for cardiac imaging has to be small enough to fit between the human ribs, and might operate in a frequency range from 2-4 MHz in order to achieve sufficient penetration to cover the heart. A transducer for imaging peripheral vessels on the other hand, can be considerably larger and might operate at frequencies of 7-14 MHz due to shallow penetration depths. The subject of transducer design is comprehensive, and out of scope for this introductory chapter. For more information on the subject please refer to [22]. Challenges for the future include the design of two-dimensional arrays for high-quality 3-D imaging, and broadband designs for multi-frequency operation and non-linear imaging.

Front-end

The front-end of the ultrasound system consists of dedicated hardware for controlling the transmission and reception of ultrasonic waves. The delays needed to focus the ultrasound beam in a given direction are calculated and used to transmit ultrasound pulses in directions according to the given scanning mode. After transmission, the system enters receive mode. Depth dependent preamplification is needed to exploit the full dynamic range of the A/D convertors. The received signal from the transducer elements are then beamformed in a given direction by a delay-and-sum procedure. A receive filter matched to the bandwidth of the received signal is applied to maximize the signal-to-noise ratio. Since the attenuation of ultrasound is frequency dependent, the receive filter is often swept to follow the changes in frequency content over depth. Echoes from deeper structures are attenuated more than echoes from shallow structures, and to image both near and far echoes simultaneously, a depth dependent amplification is applied to the signal, called time-gain compensation. The beamformed signal finally goes through a complex demodulator, where the RF-signal is transferred to baseband, and downsampled to reduce the amount of data for later processing. Much of the signal processing has in modern systems been moved to the back-end of the system, however it is also common to use dedicated hardware for this purpose in the front-end.

Back-end

In modern systems the back end of an ultrasound system typically consists of a conventional desktop computer, and is responsible for tasks such as user interfacing, signal processing, image preparation and scan conversion, and archive storage of ultrasound recordings. In modern systems, the back end tasks are performed in software running on a real-time aware operating system. User interface tasks are typically first administered by the back end. For instance, the selection of a specific image modality by the user, will first be administered by the back end computer, which further communicates with and sets up the front-end for new operation. The rapid development of computer technology has moved increasingly more tasks to the back-end of the system. Processing tasks such as image filtering, Doppler processing, and scan conversion are now feasible to do in software, which is much more flexible and cost effective than previous hardware solutions. The development of high performance graphics cards in recent years, have also made real-time rendering of 3-D ultrasound images feasible at a low cost. Systems for research are now available where beamforming can be done in software. In the long run, even real-time beamforming in software will most likely become feasible.

2.1.4 Ultrasound image quality

Spatial resolution

The spatial resolution is defined as the minimum spacing between targets that still can be distinguished by the imaging system. In ultrasound imaging the spatial resolution is theoretically given by the center frequency and bandwidth of the emitted pulse, the aperture diameter, and the focus depth. The theoretical radial resolution is related to the temporal length of the emitted pulse through the following relation:

$$\Delta r = \frac{c \cdot T_{pulse}}{2} = \frac{c}{2 \cdot B_{pulse}}, \quad (2.7)$$

where B_{pulse} is the pulse bandwidth. The radial resolution is at first hand limited by the transducer bandwidth, and is further degraded by frequency dependent attenuation which shifts the frequency contents of the received pulse towards zero. In B-mode imaging the radial resolution is in the range of wavelengths, while in Doppler modes it is increased to achieve sufficient sensitivity to the weaker blood signal level. The lateral resolution is given by a beam width measure as defined in (2.4), and is therefore dependent on the ratio between the focus depth and aperture (the F-number), and the wavelength of the emitted pulse. The lateral image resolution is broadened outside of the beam axis focus.

The total imaging system resolution can be described through the point spread function (PSF), which is defined as the image of an infinitely small point. In Fig. 2.7, the pulse-echo point spread function for pulse center frequency of 2.5 MHz with a relative bandwidth of 60%, using a F-number of 2 on both transmit and receive is shown. As can be observed in the figure, the ultrasound imaging system has a limited region of support in the Fourier space. In the lateral direction, the imaging system

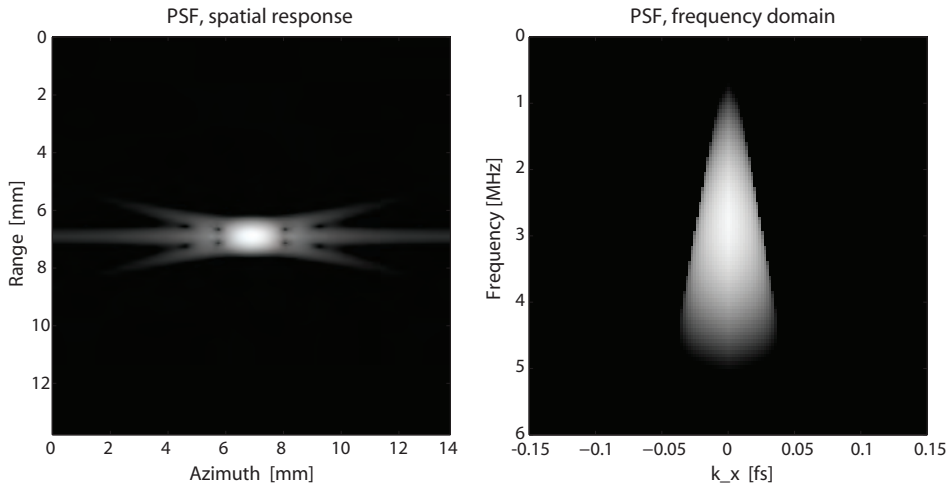


Figure 2.7: Example of a two-way point spread function (PSF) of an ultrasound imaging system. The PSF is given in focus of a transducer using an F-number of 2 on both transmit and receive. A pulse with center frequency of 2.5 MHz with a relative bandwidth of 60% was used.

exhibits a low-pass character, while in the axial direction a bandpass character is given. It is this bandpass character that gives the speckle pattern and anisotropic properties of the ultrasound images [25].

Contrast resolution

The contrast resolution is defined as the ability of the imaging system to differentiate between two regions of different scattering properties. In ultrasound imaging these scattering properties are given by local changes in compressibility and density. The contrast resolution in ultrasound imaging is degraded by beam sidelobes and by acoustic noise such as reverberations and phase front aberrations. The contrast resolution is a local characteristic, and depends both on system design and the imaging object through the inferred acoustic noise. It is therefore difficult to give an absolute measure of this property for ultrasound imaging.

Factors corrupting image quality

Several factors limit the quality in ultrasound images. These are related to both fundamental physical phenomenons and to system design.

Reverberations: Conventional ultrasound imaging operates in the Born approximation regime, where only one scattering process is assumed before the wave is received at the receiving transducer. In reality, the ultrasound wave may be scattered multiple times across its path, called reverberations. Due to

reverberations, signal from specific scatterers are received multiple times, and ghost images are there produced that degrade the contrast resolution of the image.

Phase front aberrations: In conventional ultrasound imaging, the tissue medium is assumed homogenous, and the speed of sound therefore assumed constant. In reality, different types of tissue are present with varying speeds of sound. When different parts of the beam wavefront travel through different types of tissue, the varying speed of sound will cause the wavefront to be distorted. This is termed phase front aberration. Phase front aberration infers a less efficient focusing, which result in a degradation in lateral resolution due to a broadened main lobe, and in contrast resolution due to an increased side lobe level.

Frequency dependent attenuation: Due to the frequency dependent characteristics of the attenuation of ultrasound in tissue, the received signal center frequency will shift towards lower frequencies during propagation. This center frequency shift results in a degradation of the spatial resolution and penetration which is aggravated for increasing depths.

Beam sidelobes: Due to the finite aperture used when imaging, beam sidelobes will be present. Scatterers present in the beam side lobes will be registered on receive, and in effect degrades the contrast resolution of the image. By using apodization of the individual elements on the transducer array, it is possible to trade a wider mainlobe for a lower sidelobe level.

Grating lobes: Due to the division of the aperture in array elements the beam pattern will be reproduced periodically in space. The angle between the grating lobes and the main lobe is determined by the size of the individual array elements, called the pitch. Grating lobes may infer visible image artifacts, and degrade the contrast resolution as for beam sidelobes.

2.1.5 Ultrasound Doppler imaging

When a transmitted ultrasound wave is reflected from a moving scatterer, the wave will experience a shift in frequency. This is termed the Doppler effect, named after Christian Doppler who first described the phenomenon [26]. The Doppler effect plays with our sense of time by contracting or expanding the timescale of waves as they are emitted from a moving source or reflected of a moving target. In ultrasound pulse-echo imaging both of these cases occur. The scaling of the temporal axis can then be shown to be given by [27]

$$\alpha = \frac{c + v \cos \theta}{c - v \cos \theta} \approx \left(1 + \frac{2v \cos \theta}{c}\right), \quad (2.8)$$

where θ is the angle between the scatterer velocity vector and the ultrasound beam direction, and $v \cos \theta$ is the axial component of the scatterer velocity, defined as positive towards the ultrasound transducer. The corresponding shift in frequency is then given

by:

$$f_d = \alpha f_0 - f_0 = 2f_0 \frac{v \cos \theta}{c}, \quad (2.9)$$

where, f_d is termed the Doppler shift, and f_0 is the emitted frequency. The equation is valid as long as $v \cos \theta \ll c$.

The Doppler principle can be used to measure the velocity of both tissue and blood with ultrasound. Tissue velocities are typically quite low compared to blood flow, but with some exceptions. The contractions of the myocardium can for instance be in the range around 10 cm/s, while the movement of the heart valves can have velocities as high as 50 cm/s. For blood flow the velocities range up to 1 m/s for normal flow, while stenotic and valve insufficiency flow can reach as high as 6 m/s. Imaging with a pulse center frequency of 2.5 MHz, this means that Doppler shifts can range up to 19500 kHz. In diagnostic ultrasound, the Doppler shifts are hence in the human audible range.

For blood the received signal from an insonified sample volume is a sum of contributions from a large number scatterers, each producing a Doppler shift according to their given velocity and direction. The received signal is therefore made up of a spectrum of different velocities. Further, as each scatterer is observed in a finite time interval, a non-zero bandwidth is given for each velocity. This is termed the transit time effect.

The velocity spectrum within a sample volume can be investigated by spectral analysis of the received signal. As the Doppler shift is in the audible range, it is also common to generate sound through a set of speakers for the physicians to interpret. This was in fact how the early Doppler instruments strictly operated, before real-time spectral analysis became computationally feasible. An increasing scatterer velocity causes an increasing Doppler shift and therefore a higher pitch of the sound. Two different Doppler modalities have become standard, based on either a continuous wave (CW) excitation, or a pulsed wave (PW) excitation approach. A brief description will now be given. For a more thorough description please refer to [21, 22, 27, 28].

Continuous-wave Doppler

In continuous-wave Doppler (CW-Doppler), a single frequency signal is continuously transmitted into the tissue, while the backscattered signal is simultaneously received, typically by a different parts on the same transducer aperture. The sample volume in CW-Doppler is given by the overlap between the transmit and receive beam. Doppler shifts from all scatterers moving in this large region of overlap are therefore observed, and in practice no range resolution is available in CW-Doppler. The main advantage of the CW approach is that it is not limited by a maximum measurable velocity, as a continuous recording of the Doppler signal is obtained.

The magnitude and sign of the Doppler frequency can be obtained by quadrature demodulation. Consider the CW emission given by

$$e(t) = \cos(2\pi f_0 t) = \text{Re}\{e^{i2\pi f_0 t}\}, \quad (2.10)$$

where f_0 is the emitted sinusoidal frequency. Assuming the received signal at time t to be a delayed, scaled, and Doppler shifted version of the emitted signal at time t_0 , we get:

$$r(t) = A(\alpha(t - t_0)) \cdot e(\alpha(t - t_0)) = A(\alpha(t - t_0)) \cdot \cos(2\pi f_0 \alpha(t - t_0)). \quad (2.11)$$

The complex analytic signal can be obtained through the Hilbert transform, and is given by:

$$\tilde{r}(t) = \tilde{A}(\alpha(t - t_0)) \cdot e^{i2\pi\alpha f_0(t-t_0)} \quad (2.12)$$

Mixing the received analytic signal with the quadrature reference signal $e^{-i2\pi f_0 t}$ then yields:

$$\begin{aligned} r_{IQ}(t) &= \tilde{A}(\alpha(t - t_0)) \cdot e^{i2\pi\alpha f_0(t-t_0)} \cdot e^{-i2\pi f_0 t} \\ &= \tilde{A}(\alpha(t - t_0)) \cdot e^{i2\pi(\alpha f_0 - f_0)t + 2\pi f_0 t_0} = \tilde{A}(\alpha(t - t_0)) \cdot e^{i2\pi f_d t + \phi_0}, \end{aligned} \quad (2.13)$$

revealing the complex Doppler signal.

Pulsed-wave Doppler

In pulsed-wave Doppler (PW-Doppler), a series of pulses are emitted into the tissue at a constant pulse repetition frequency (PRF), phase-coherent with respect to the transmission carrier frequency f_0 , and range-gated on receive to achieve range resolution as in regular pulse-echo imaging. As the pulses interact with moving scatterers, they are reflected and shifted in frequency according to (2.9). In PW-Doppler, the pulse length need to be shorter than $T = 1/PRF$ in order to achieve range resolution. This requirement and the fact that the change in pulse bandwidth due to attenuation can be large compared to the Doppler shift itself, makes it difficult to measure the Doppler shift directly as in CW-Doppler [27]. Instead, an approach based on analyzing the difference in subsequently emitted pulses is taken. Due to the axial movement of the scatterer, the received signal from consecutive emissions will be delayed an amount proportional to the axial velocity. A simplified example for a single scatterer will illustrate this. The emitted pulse typically consist of a burst of sinusoidal oscillations, as given in complex form by

$$e(t) = g(t)e^{i2\pi f_0 t}, \quad (2.14)$$

where $g(t)$ is the complex envelope of the pulse and f_0 is the pulse carrier frequency. Given a single scatterer at depth r_0 with velocity v and angle θ compared to the ultrasound beam. Pulses are emitted at intervals of T seconds. The received complex signal from a pulse emitted at time t can then be described by

$$r_m(t) = e(\alpha(t - t_m)), \quad (2.15)$$

where α is the time compression factor given in (2.8), and t_m is the relative time from pulse emission to reception for pulse number m , given by

$$t_m = \frac{2r_0}{c} + \frac{2v \cos \theta m T}{c} = t_0 + m\tau. \quad (2.16)$$

The relation between two consecutive pulses then becomes

$$r_m(t) = e(\alpha(t - t_m)) = e\left(\alpha(t - t_0 - \frac{2v \cos \theta m T}{c})\right) = r_{m-1}(t - \tau), \quad (2.17)$$

which in this ideal case is a delayed version of the previous pulse, given by the displacement of the scatterer in the axial direction. The velocity of the scatterer can be found either by trying to estimate τ directly from consecutive RF-signals, or by sampling the resulting change in phase compared to the carrier frequency between consecutive pulses. Conventional PW-Doppler uses the latter method. Inserting (2.14) into the expression for $r_m(t)$ gives

$$r_m(t) = g(\alpha(t - t_m))e^{i2\pi f_0 \alpha(t - t_0 - m\tau)} = g(\alpha(t - t_m))e^{i2\pi f_0 \alpha(t - t_0)}e^{i\phi(m)}, \quad (2.18)$$

where the additional phase function $\phi(m)$ is given by

$$\phi(m) = 2\pi f_0 \alpha \frac{2v \cos \theta T}{c} m. \quad (2.19)$$

The frequency of this phase function then becomes

$$f_\phi = \frac{1}{2\pi} \frac{\phi(m) - \phi(m-1)}{T} = 2f_0 \alpha \frac{v \cos \theta}{c} \approx f_d, \quad (2.20)$$

where the instantaneous frequency is approximated by a discrete derivative. As seen, the instantaneous Doppler shift is actually an artifact in pulsed Doppler systems. The equation is valid for $v \cos \theta \ll c$. This signal is termed the complex Doppler signal, or simply the Doppler signal. In practical systems, the complex Doppler signal is obtained by removing the carrier frequency through complex demodulation. The sign of the Doppler shift can be obtained by inspecting the phase relationship between the in-phase and quadrature components [20, 21].

2.2 Color Flow Imaging

2.2.1 Background

Color flow imaging (CFI) is a modality that provides an image of flow velocity and direction in a two- or three-dimensional region of interest. In this way, the distributed flow presence throughout an image region can be observed, abnormal flow patterns can be detected and investigated, and quantitative measurements of flow velocities can be combined with area estimates to produce volume flow. The information acquired by CFI is encoded in a color image, hence its name, and is combined with B-mode imaging of tissue to provide an image both the tissue anatomy and flow conditions. The modality has been given different names, and other well used synonyms and acronyms include color flow mapping (CFM) and color-Doppler imaging (CDI), the latter is most often used in the clinical community.

In today's high-end ultrasound systems, the CFI modality is integrated along with B-mode and M-mode imaging, and also PW- and CW-Doppler modes. Duplex and

triplex imaging where combinations of the modalities are also available. The CFI modality both alone and in combination with spectral Doppler has proven valuable in many different clinical contexts, such as in cardiology, obstetrics and gynecology, pediatrics, vascular surgery, and more [18, 19]. The method has perhaps found particular use in the diagnosis of the cardiovascular system, where it for instance is used to locate and evaluate heart valve insufficiencies, septum defects, and artery plaque stenosis.

Color flow imaging provides quantitative measurements of the axial velocity and direction of blood flow. However, the method is despite of this mostly used in a qualitative way for the visual detection of areas of abnormal blood flow patterns. These areas are then further examined using the more detailed spectral display of CW- and PW-Doppler. The reason for the non-quantitative use can be related to basic limitations in temporal resolution of the velocity measurements compared to the spectral Doppler techniques, but can also be attributed to limitations of current estimation schemes with regards to velocity aliasing and angle-dependencies.

The history of ultrasound CFI began in the late seventies, when multi range gate (MRG) PW systems were introduced to estimate the flow velocity along several range gates in depth [29]. This allowed for the measurement of velocity profiles. The concept of color flow imaging emerged as a natural extension of these MRG PW instruments, by also estimating the flow velocity along several beams directions. The first two-dimensional color flow images were produced by processing data from MRG Doppler system scanned over a region of interest [30, 31].

The estimation of the complete Doppler spectrum in each range gate is an unpractical solution in CFI, and research efforts was put into finding efficient and accurate algorithms for estimating representative spectral parameters such as the mean Doppler frequency. This approach had previously been abandoned in the context of PW-Doppler systems when real-time spectral processing became feasible [32], but was once again a relevant issue for MRG Doppler and CFI methods. In CFI the estimation procedure is particularly challenging due to short ensemble lengths available for processing. Time-domain algorithms became the practical solution, and several estimators were proposed for real-time estimation of the first three spectral moments, signal power, mean frequency, and frequency spread in the CFI context [32–35].

The first real-time CFI systems were introduced in the mid-eighties. They were based on the autocorrelation approach introduced to the ultrasound community by Namekawa and Kasai [36, 37]. The method had earlier been described and used in the weather-RADAR community [38–40], where real-time color-Doppler imaging was demonstrated as early as the mid-seventies [41]. The autocorrelation estimator has prevailed, and is today the standard algorithm used in most commercial scanner systems. Since the first real-time systems, the modality has been improved in different aspects. The first commercial system was actually based on electronic scanning using phased-array transducers. However, the potential of electronic scanning could not be fully exploited for CFI at this time, and mechanically scanned transducer systems were soon after introduced with better performance. It was first by the advent of digital front-end technology that the advantages of electronic scanning really could be utilized through beam interleaving and parallel beamforming techniques,

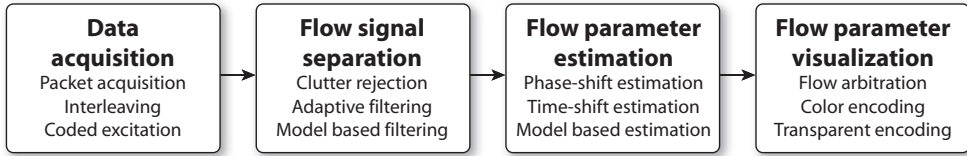


Figure 2.8: Block diagram of basic CFI processing.

increasing the flexibility and frame rate. Digital systems have further eased the implementation of new algorithms, for instance the implementation and evaluation of more advanced clutter rejection filtering, which has received much attention due to its major influence on the resulting images. The computational power of today's desktop computers are now at a stage where the CFI processing can be done in software, which further increases the flexibility. The latest technology to appear is real-time dynamic three-dimensional color flow imaging based on data acquired using 2-D phased-array transducers. This modality take full advantage of the increased processing power of current CPUs, and also the massive development in graphic card performance that has taken place in recent years, making it possible to do real-time three-dimensional rendering of image volumes.

In the following subsections, a detailed look at the inner workings of CFI systems will be given, and some aspects not covered in the thesis papers will also be included. An in-depth description of CFI systems and algorithms has also been given by Jensen [27], Angelsen and Torp [42], Wells [43], and Ferrara [44]. Detailed descriptions of clinical application of CFI can for instance be found in [18, 19, 21].

2.2.2 Building blocks of ultrasound CFI

A block diagram illustrating the basic signal processing blocks of CFI is given in Fig. 2.8. At each processing stage in the figure, a number of subtopics are listed which will be explained in coming sections. The processing described is based on the assumption of using transducer arrays, where the ultrasound beam can be steered and focused electronically in the desired directions. In this way subsequent beams has discrete positions in space, which is contrary to mechanical transducers where the beam is swept continuously over the image region of interest. After the data acquisition of a complete CFI frame, N_P discrete number of temporal samples is available for processing for each sample bin in the image. This temporal signal vector \mathbf{x} is first processed to remove the clutter signal from tissue structures, which is referred to as the blood signal separation stage. After the separation of the blood flow signal, the estimation of parameters reflecting properties of the flow is performed. Typically, the mean velocity of blood scatterers, the blood signal power, and also the blood velocity spread within the sample volume is estimated. The estimated parameters are conventionally encoded in different colors and visualized superimposed on a gray-scaled B-mode image of the tissue anatomy. The CFI processing will now be described in more detail.

2.2.3 Data acquisition

The data acquisition in CFI is based on a pulsed wave approach. The ultrasonic beam is scanned over the region to be imaged, and a series of N_P pulses are transmitted and received in each beam direction. This acquisition scheme is referred to as packet acquisition, and the number of pulses N_P is called the packet size. There are several challenges in CFI acquisition. Blood flow parameters are estimated for every range gate along the beam. To investigate local changes in the two-dimensional velocity distribution, a high spatial resolution and therefore the use of high-bandwidth pulses are desired. However, assuming the pulse energy constant, the signal-to-noise ratio of the received signal from blood can be shown to be inversely proportional to the bandwidth of the emitted pulse [45], and to achieve a sufficient sensitivity, longer pulses must most often be used. This compromises the spatial resolution, and also requires a separate acquisition of B-mode images. If the acoustic energy of the emitted pulse is limited by restrictions set on the emitted pulse amplitude, one way to retain both a high spatial resolution and sufficient sensitivity could be to use coded excitation [46, 47]. For instance, a longer pulse with high bandwidth such as the chirp excitation could be transmitted, and deconvolved on receive for pulse compression.

Another challenge is that of frame rate. In order to achieve a good separation of the blood flow signal component and high quality velocity estimates, it is desired to have a high packet size. However, in order to follow the dynamics of the flow, a high imaging frame rate is required. This restricts the packet size to typically 8-16 samples depending on the clinical application. The frame rate can be increased by reducing the lateral beam sampling, however this will reduce the spatial resolution and therefore the quality of the image, and a compromise is again made. In modern scanner systems, multi-line acquisition (MLA) is often available, where several receive beams are generated per transmit beam, increasing the frame rate at the expense of more beamforming hardware [48, 49]. With the introduction of real-time 3-D color flow imaging using 2-D arrays, the problem of frame rate has become even more critical. More MLA could be performed, but these methods also introduces image artifacts. The number of MLA is also limited by demands of sensitivity, as a broader transmit beam must be used.

The received signal along each beam is sampled throughout the image depth at a high sampling rate (~ 50 MHz) and is referred to as the fast-time signal. For a given range depth, the signal formed from subsequent beam acquisitions is referred to as the slow-time signal. This concept is shown in Fig. 2.9, illustrating the received and beamformed signal along a direction containing a strong stationary scatterer at z_0 , a moving scatterer at z_1 , and a thermal noise component. Combined, the fast-time and slow-time signal from a given range gate form the complete signal foundation of CFI velocity estimators. The corresponding Fourier space content is shown to the right. As can be seen, the blood flow signal of interest is spread in two frequency dimensions. The angle ϕ is related to the velocity of the scatterers through the Doppler equation.

The rate of subsequent pulse transmissions, the pulse repetition frequency (PRF), determines the sampling rate of the slow-time signal. The slow-time signal variation must therefore lie below $\text{PRF}/2$, the Nyquist rate, in order to be properly represented.

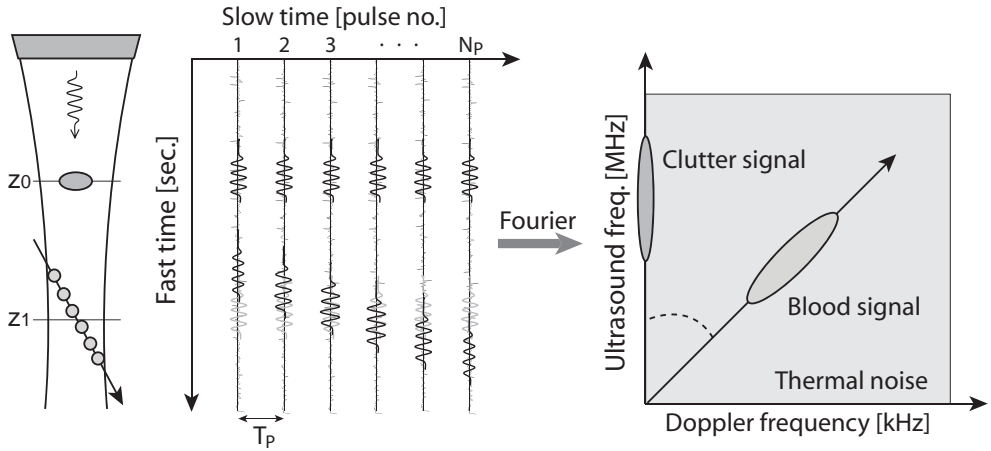


Figure 2.9: Input signal foundation for processing in CFI. In the example a strong scatterer one dimension along the beam called fast-time, and one between subsequent beams called slow-time. To the right the two-dimensional Fourier transform depict

For velocity estimators utilizing the slow-time signal only, the PRF used is therefore proportional to the maximum velocity measurable before aliasing occurs. The depth of the image scan determines the maximum PRF available before ambiguities as to where the signal is obtained is introduced. Although this constraint is sometimes disregarded in high-PRF Doppler modalities, it is avoided in conventional CFI by waiting the appropriate time before firing a new pulse. By decreasing the PRF with a factor k , there is time to acquire data in $k-1$ other beam directions before transmitting the next pulse in the initial direction. This technique is termed beam interleaving [50]. The k number of beams is called the interleave group size (IGS) and together form an interleave group (IG). The interleave group size (IGS) can be expressed by

$$\text{IGS} = \left\lfloor \frac{\text{PRF}_{\max}}{\text{PRF}} \right\rfloor \cdot \text{MLA}, \quad (2.21)$$

where MLA is the number of parallel receive beams acquired, and $\lfloor \cdot \rfloor$ means rounding off to the nearest integer towards $-\infty$. Beam interleaving is used to maximize the overall frame rate for a given user chosen PRF, set according to the blood velocity range of interest.

After beamforming and complex demodulation of the received signal has been performed, the signal-to-noise ratio (SNR) of the received signal is maximized by a filter matched to the received signal bandwidth. It has been shown that using a receive filter with a rectangular impulse response with length equal to the emitted pulse is close to optimal for this purpose [45].

2.2.4 Signal model

General signal model

After data acquisition, a two-dimensional signal matrix is in general given, consisting of sampled data in both fast-time and slow-time respectively, as illustrated in Fig. 2.9. In this thesis work, only the slow-time signal is considered, which means that the signal from each range gate is processed separately. The resulting received signal then reduces to a complex signal vector of N_P slow-time samples, $\mathbf{x} = [x_1, x_2, \dots, x_{N_P}]^T$.

The received slow-time signal from an insonified sample volume is in our general model assumed to consist of three signal components. A clutter component \mathbf{c} originating from sound scattered from tissue and acoustic noise sources such as reverberation and beam side lobes, a blood signal component \mathbf{b} originating from sound scattered from the moving blood cells, and an electrical/thermal noise component \mathbf{n} . The general signal model is then given by

$$\mathbf{x} = \mathbf{c} + \mathbf{b} + \mathbf{n}. \quad (2.22)$$

The blood and clutter signal components originate from different scattering sources at different spatial locations, and are therefore considered statistically independent. As the bandwidth of the thermal noise after receiver filtering is large compared to the sampling frequency of the Doppler signal (PRF), it is modeled as white noise.

Assuming a zero-mean complex Gaussian process for the received signal from both blood and tissue as rationalized in the upcoming Section 2.2.4 and 2.2.4, the probability density function (PDF) of the received signal vector is given by

$$p_{\mathbf{x}}(\mathbf{x}) = \frac{1}{\pi^N |\mathbf{R}_{\mathbf{x}}|} e^{-\mathbf{x}^* \mathbf{R}_{\mathbf{x}}^{-1} \mathbf{x}}. \quad (2.23)$$

Being Gaussian, the signal is completely characterized statistically by its second order moments. The second order moment information is then contained in the signal correlation matrix given by [51]

$$\mathbf{R}_{\mathbf{x}} = \text{E}\{\mathbf{x}\mathbf{x}^* \mathbf{T}\}, \quad (2.24)$$

where E denotes the expectation operator. Assuming statistical independence this can further be written as

$$\mathbf{R}_{\mathbf{x}} = \mathbf{R}_{\mathbf{c}} + \mathbf{R}_{\mathbf{b}} + \mathbf{R}_{\mathbf{n}} = \mathbf{R}_{\mathbf{c}} + \mathbf{R}_{\mathbf{b}} + \sigma_n^2 \mathbf{I}, \quad (2.25)$$

where $\mathbf{R}_{\mathbf{c}}$ is the clutter correlation matrix, $\mathbf{R}_{\mathbf{b}}$ is the blood signal correlation matrix, σ_n^2 is the thermal noise variance, and \mathbf{I} is the identity matrix. In this framework we do not assume stationarity.

Blood signal model

Blood is a medium consisting of several types of cells suspended in a fluid medium known as plasma. The main cell concentration is made up of red blood cells (RBCs),

or erythrocytes. The scattering medium in the blood plasma is mainly these red blood cells, which have a diameter of about $6 - 8\mu m$ [52]. As the scattering size is much smaller than the wavelength used in medical ultrasound imaging, the scattering properties will exhibit Rayleigh characteristics. This means that the sound scattered from blood follows a frequency dependency law for the scattering power of f^4 .

There are two main approaches for modeling the blood medium and its ultrasound scattering characteristics. One approach models the blood as a large collection of particle objects [53, 54]. The main advantage of this approach is that the principle of superposition can be applied to sum the backscattered wavelets from each individual RBC. Another approach models the blood as a random continuum, where the insonified scattering volume is assumed to consist of many scattering RBCs, which together form a continuum whose density ρ and compressibility κ change due to fluctuations in blood cell concentration, causing the scattering of incoming ultrasound pressure waves [52, 55]. The two models can explain different properties known to exist for the scattering of blood, but neither are consistent with measurements of the backscattering coefficient in presence of phenomena such as turbulence, shear rate, and varying hematocrit [56, 57]. A unified approach where a hybrid of the two models have also been proposed to provide a higher level of accuracy [58]. A more thorough review of the different models proposed is also given here. There is a general agreement in both models, that the scattering of ultrasound from blood can be described as a zero-mean Gaussian process due to the large number of scattering red blood cells within an ultrasound resolution cell. Considering the complex demodulated signal, a corresponding complex Gaussian process is given.

The Doppler signal received from blood flow depends on the direction and velocity relative to the ultrasound beam of all scatterers in the ensemble present within a resolution cell. Each scatterer contributes to the total receive signal with a Doppler shift, and a finite Doppler bandwidth due to the limited observation time related to the movement through the sample volume. Turbulent behavior of flow will increase the Doppler signal bandwidth.

By assuming rectilinear motion, and Gaussian shaped beam profiles constant over the pulse shape, the received Doppler spectrum can also be shown to be Gaussian shaped [59].

Tissue signal model

Tissue consist of different types of scatterers of varying size compared to the wavelength of the transmitted ultrasound pulse, and therefore exhibit different scattering characteristics. The scattering properties may further also vary with the angle of insonification. Such anisotropy can be observed for instance when imaging muscle fibers in the ventricle septum of the heart [25, 60]. Tissue characterization based on analysis of the backscattered pressure waves from ultrasound has been an area of research since the birth of diagnostic ultrasound imaging [5], but is still considered experimental.

A simplified view is taken in this work. It is well known, that when the ultrasound field insonifies a volume containing a large amount of randomly distributed scatterers,

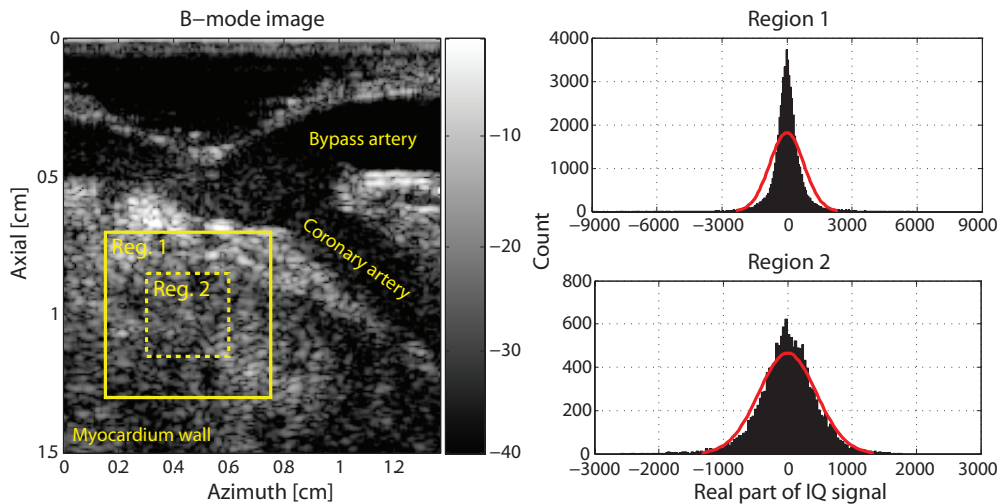


Figure 2.10: The tissue signal histogram from two different regions in the myocardium wall of a pig. As can be observed, when looking at smaller regions, the distribution of the tissue signal approaches a Gaussian shape. The data was acquired using an i13L linear array (GE Healthcare, WI, USA) with a pulse frequency of 14 MHz.

a Gaussian distributed signal results [61]. This results in what is called fully developed speckle in the ultrasound images. In parts of this thesis work where a tissue model is applied, we assume this to be the case. When considering larger regions with non-uniform scattering, a non-Gaussian distribution of the received tissue signal is typically given due to large differences in scattering strengths. It can be justified however, that when looking smaller regions in an image where a close to uniform medium is given, the distribution of the received signal from tissue approaches a Gaussian shape. An example of this is shown in Fig. 2.10, where the myocardium wall of a pig is imaged using an i13L linear array probe (GE Healthcare, WI, USA) operating at 14MHz. As can be observed, when looking at smaller sections of an image, the distribution of the tissue signal does in fact approach a Gaussian shape.

The Doppler signal from tissue results from tissue movement due to muscle contractions, and muscle vibrations in the operator holding the ultrasound probe and the patient. There may also be a relative motion of the probe against the patient skinline. The muscle contractions are typically cyclic, and are therefore accelerated. This acceleration will increase the bandwidth of the tissue Doppler spectrum. Tissue muscle vibrations were analyzed in [62], where it was modeled as a zero-mean Gaussian process, and shown to set a lower bound on the measurable Doppler shifts from blood.

2.2.5 Blood signal separation

Blood flow signal separation remains an important topic in CFI. Due to beam side lobes and reverberations, signal from surrounding tissue is also present inside the vessel

lumens and the ventricles of the heart. This tissue clutter signal dominates the received signal, and is a major source of bias in subsequent estimation of blood flow parameters. Regardless of parameter estimation technique, the clutter signal must be accounted for. A similar problem exist in RADAR, where fixed target canceling (FTC) is performed to remove the stationary ground clutter component by simply subtracting subsequently acquired beams, a simple high-pass filter. In diagnostic ultrasound imaging, this problem is more elaborate. The tissue clutter can exhibit a substantial movement during the heart cycle, which complicates matters by increasing the center frequency and bandwidth of the tissue Doppler signal spectrum.

In conventional CFI algorithms, the clutter signal is removed by high-pass filtering in the slow-time domain. Due to the discrete acquisition of subsequent beams, the slow-time signal vectors must be filtered separately for each beam direction. The clutter filter in CFI should have a sufficient stop-band attenuation for removing the clutter component, and a short transition region to minimize removal of the Doppler signal from blood. For most cases a stop band damping of 80 dB would be sufficient.

For clutter filtering purposes in CFI both finite impulse response (FIR), infinite impulse response (IIR) high-pass filters, and also polynomial regression filters have been used [63–66].

FIR filters

FIR filters can be described by an impulse response function $h(n)$, $n = 0, \dots, M - 1$, where $M - 1$ is denoted the filter order. With an input signal $x(n)$, $n = 0, \dots, N_P - 1$, the output signal $y(n)$ is the convolution sum given by

$$y(n) = \sum_{k=0}^{M-1} h(k)x(n - k), \quad (2.26)$$

where the first $M - 1$ output samples are invalid and discarded. FIR filters have the advantage of being time invariant and easy to implement with low computational demands. On the negative end, initializing filter samples have to be discarded, leaving fewer samples for velocity estimation. As the following correlation estimates are not dependent on the phase response, improved FIR filters for CFI can be achieved by designing a minimum-phase filter [64]. A decreased variance in subsequent estimation can then also be achieved by averaging estimates achieved after filtering in both the forward and backward direction.

IIR filters

An infinite impulse (IIR) filter can be described by the difference equation

$$y(n) = - \sum_{k=1}^M a_k y(n - k) + \sum_{k=0}^M b_k x(n - k), \quad (2.27)$$

where M is denoted the filter order. This is a recursive equation, and the output samples $y(n)$ are dependent on present and past input samples as well as past output

values. Due to the small number of samples available, the transient response of the IIR filter must be reduced on the expense of a sharp steady-state filter response. The initialization of the IIR filter therefore becomes important. Several methods have been described for the initialization of IIR filters [66–68]. It has been shown that projection initialization, where the transient vector subspace is removed from the output signal by projection is superior for CFI applications [64].

Regression filters

Polynomial regression filter models the clutter signal by a set of orthonormal slowly varying polynomial basis functions [63, 65]. Typically, the Legendre polynomials have been used. The filter output is given as the projection of the input signal vector \mathbf{x} onto the complement of the clutter signal basis given by

$$\mathbf{y} = \left(\mathbf{I} - \sum_{k=0}^{M-1} \mathbf{b}_k \mathbf{b}_k^{*T} \right) \mathbf{x} = \mathbf{A} \mathbf{x}, \quad (2.28)$$

where \mathbf{b}_k are orthonormal basis vectors spanning the clutter signal subspace, \mathbf{I} is the identity matrix and \mathbf{A} is a projection matrix. The filter order is given by $M - 1$. Polynomial regression filters have a high stop band attenuation, and an attractive transition region compared to FIR and IIR filters. Another specific advantage of regression filters is that no samples need to be discarded after filtering, reducing the variance in subsequent flow parameter estimation. A disadvantage of the polynomial regression filter approach is that it is not time-invariant. This causes a severe frequency distortion in the transition region of the filter [63].

In Fig. 2.11, the frequency response of the three different types of filters are shown for comparison. The main challenge of using high-pass filters to remove clutter in CFI is to achieve filters with sufficient stop-band attenuation and at the same time a sharp transition region for the short ensemble lengths available (see Section 2.2.3). Due to the resulting non-ideal frequency response of the filters, they have a negative impact on subsequent estimator accuracy [63, 64]. An insufficient stop-band attenuation for removing the clutter component will lead to a negative bias towards zero frequency for mean-frequency estimators. A long transition region of the clutter filter may remove parts of the blood flow component, causing a positive bias. Also, the white noise component becomes correlated after filtering, and contributes to a positive bias [69, 70].

2.2.6 Blood signal parameter estimation

In color flow imaging, the scatterer velocity is estimated by exploiting the change in the RF or baseband signal due to scatterer movement over several pulse emissions. Different approaches exist to accomplish this. The estimation of the Doppler spectrum as in PW-Doppler is not a practical solution. Few temporal samples are available and would lead to poor spectrum estimates, and the sheer amount of information would in any case be difficult to visualize properly. Instead, parameters reflecting properties

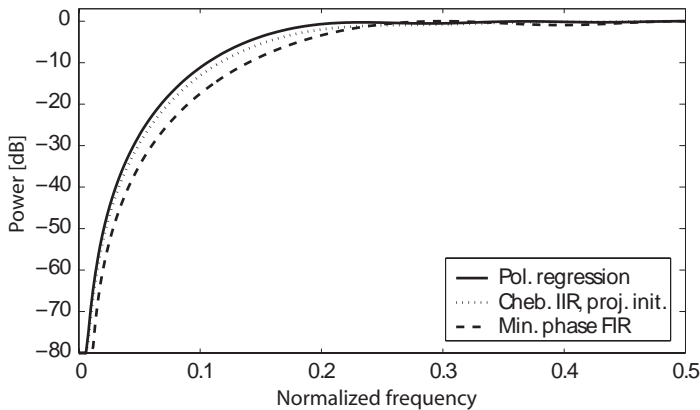


Figure 2.11: Comparison between three different types of high-pass clutter filters, a fourth order polynomial regression filter, a projection initialized Chebychev IIR filter, and a minimum-phase FIR filter. The figure is taken from [64].

of the Doppler spectrum is estimated. This process is done separately for each range bin for several beams in a region of interest.

Conventional parameters of interest in CFI are the blood flow signal power P indicating the presence of blood flow, the mean frequency of the Doppler spectrum $\bar{\omega}_d$, and also the frequency bandwidth of the Doppler spectrum B , which relates to flow disturbance. These parameters are directly related to the first three central moments of the Doppler spectrum, which for a discrete process is given by [32, 42]

$$P = \int_{-\pi}^{\pi} G(\omega)d\omega, \quad \bar{\omega}_d = \frac{1}{P} \int_{-\pi}^{\pi} \omega G(\omega)d\omega, \quad B^2 = \frac{1}{P} \int_{-\pi}^{\pi} (\omega - \bar{\omega})^2 G(\omega)d\omega. \quad (2.29)$$

Estimation of spectral moments from short ensemble lengths is a challenging task. Much work on the subject was performed in the weather-radar community in the late seventies and early eighties parallel to the development in ultrasound imaging [40, 71], where a similar problem and data acquisition is given. Implementation wise, spectral parameter estimation can be done in the frequency or time-domain. In the frequency domain an estimate of the power spectrum $\hat{G}(\omega)$ is replaced for $G(\omega)$ in (2.29). This is however not a practical solution in CFI due to computational demands. Time-domain estimators obtain spectral parameters directly from the signal samples or through correlation analysis, and can have low computational demands.

The estimators are further characterized based on the signal information they employ. Referring to Fig. 2.9, the slow-time signal only or both the slow- and fast-time signal can be utilized. The estimators are also characterized as being either narrow or wide band estimators, based on the validity and assumption of input signal bandwidth. Narrow band estimators are in principle valid for single frequency signals, or may degrade in presence of wide band pulses, while wide band methods are valid for general wide band pulse emissions.

Phase-shift estimation is based on the fact that a displacement of the blood scatterers between pulse emissions can be related to a change in phase of the received signal compared to the demodulation frequency. Phase-shift estimation is limited by aliasing when the displacement of scatterers correspond to a phase-shift of more than $\pm\pi$. Basic phase-shift estimation utilize the slow-time signal only and are typically narrowband. Phase-shift techniques have low computational demands, and can also be done efficiently in the base-band.

Time-shift estimation is based on estimating the time delay of the received echoes due to the displacement of scatterers, tracking the scatterer movement in the received RF-signal. Methods include cross-correlation of subsequent pulse emissions, and Fourier based methods implemented in time domain. Model based methods have also been proposed. Time-shift estimation techniques exploit both the slow- and fast-time information, and therefore produce estimates with a lower bias and variance, and also above the aliasing limit. The improved performance may become marginal when longer pulse lengths are needed to achieve sufficient penetration. Time-shift estimation algorithms are in general much more computationally demanding than phase-shift algorithms. Also, when based on RF-data this complexity is further increased.

Several specific estimators have been proposed for the estimation of blood flow velocity in CFI. In the following subsections, a brief review of some of the most important velocity estimators will be presented. The techniques described here deals with the estimation of the axial velocity component. Experimental methods that also estimate the lateral velocity component have been given a specific review in Section 2.4.

The autocorrelation estimator

The autocorrelation estimator was the one used to first demonstrate the feasibility of real-time two-dimensional ultrasound color flow imaging. It was introduced by Nakemawa and Kasai for diagnostic ultrasound applications in the mid-eighties [36, 37], but was earlier described in the context of weather radar by several authors [38–40], where it eventually was named the correlated pulse-pair estimator.

The autocorrelation approach estimates the three spectral parameters P , $\bar{\omega}_d$ and B from the slow-time correlation function $R_x(m)$ at lag zero and one, given by

$$\hat{P} = \hat{R}_x(0), \quad \hat{\omega}_d = \angle \hat{R}_x(1), \quad \hat{B} = \sqrt{1 - \frac{|\hat{R}_x(1)|}{\hat{R}_x(0)}} \quad (2.30)$$

A simple view of of the autocorrelation mean frequency estimator can be given as follows. The correlation function $R_x(m)$ is related to the Fourier transform of the Doppler spectrum through the Wiener-Kinchin theorem, which for $m = 1$ is given by

$$R_x(1) = \frac{1}{2\pi} \int_{-\pi}^{\pi} G(\omega) e^{i\omega} d\omega = \frac{e^{i\bar{\omega}_d}}{2\pi} \int_{-\pi}^{\pi} G(\omega) e^{i(\omega - \bar{\omega}_d)} d\omega. \quad (2.31)$$

As can be seen, the mean Doppler frequency $\bar{\omega}_d$ can be estimated from the phase angle of $R_x(1)$ if the imaginary part of the last integral in (2.31) is zero. This is the case

for spectra that are symmetric around the mean frequency [40], but is also a good approximation for narrowband spectra.

In practise, the autocorrelation function of lag one is estimated from the received signal sequence $\hat{R}_x(1)$. The mean axial velocity of blood is further obtained by a scaling factor

$$\hat{v}_z = \frac{c \cdot PRF}{4\pi f_0} \angle \hat{R}_x(1) \quad (2.32)$$

The properties of the autocorrelation estimator have been examined by several authors, both in the weather radar community [38–40], and in the context of ultrasound blood velocity estimation [35, 59, 72]. The autocorrelation estimator has been shown to be an unbiased estimator of the mean spectral frequency for symmetric spectra, and in presence of white noise, and can further estimate the mean frequency over the whole frequency range from $-\pi$ to π . When utilizing spatial averaging the autocorrelation estimate has been shown to improve substantially [72]. The autocorrelation approach has also been extended to also use the fast-time signal through the simultaneous estimation of the mean fast-time frequency [73], which was shown to reduce the variance of the velocity estimates.

The cross-correlation estimator

The cross-correlation estimator has also received much attention for blood flow velocity estimation in diagnostic ultrasound. The concept of cross-correlation estimation of blood flow velocity is in principle quite simple. As shown in Section 2.1.5, the received signal from subsequent beam emissions is delayed a given time τ due to the scatterer movement, given by

$$\tau = \frac{2\Delta z}{c} = \frac{2v \cos \theta T}{c}. \quad (2.33)$$

This time delay can be estimated by finding the point of maximum correlation between subsequent pulses r_1 and r_2 in a range segment, given by

$$\hat{\tau}_{max} = \arg \max R_{12}, \quad (2.34)$$

where the cross-correlation for a specific range segment in the RF-signal is estimated discretely by [27]

$$\hat{R}_{12}(m) = \frac{1}{N_S} \sum_{k=0}^{N_S-1} r_1(k)r_2(k+m), \quad (2.35)$$

where N_S is the number of range samples in a given range segment. Knowing the time between pulse emissions T_P , the axial velocity estimate can be calculated from

$$\hat{v}_z = \frac{c \hat{\tau}_{max}}{2 T_P}. \quad (2.36)$$

As the velocity estimate produced by the cross-correlation technique is related to the lag of maximum correlation, it is the dominant scatterer movement that is being

tracked. The method can therefore not in general be related to the mean velocity of the ensemble insonified as the autocorrelation technique.

The cross-correlation technique applied for ultrasound blood flow velocity estimation, was described amongst others by Bonnefous [74], Foster [75], and Embree and O'Brian [76], and has been validated both in-vitro and in-vivo. The influence of different imaging system parameters on the delay estimate was described in [75]. The technique can achieve a lower variance estimate of the axial blood velocity compared to the autocorrelation approach, and is in theory not limited by aliasing. However, signal decorrelation sources will degrade the performance. The increased performance compared to the autocorrelation method is reduced when longer pulses must be used to obtain sufficient sensitivity. When also utilizing radial averaging in the autocorrelation technique, the performance of the two has been shown to be comparable in certain contexts [77].

Other estimators

Other estimators have been proposed since the introduction of real-time color flow imaging. Ferrara and Algazi proposed a wideband maximum likelihood estimator [78], based on a model of a slowly fluctuation range-spread target. In this approach the received signal is matched filtered to a model of the received signal of varying parameters, and parameter estimates are determined from the best match. Other wideband tracking techniques have been also proposed by Wilson [79] and Kaisar and Parker [80]. A different approach was taken by Vaitkus who proposed using a root-MUSIC estimator in CFI [81]. This estimator is based on the modeling of the blood and clutter signal components as a number of eigenvectors of the estimated signal correlation matrix. Similarly, AR modeling of the Doppler signal in CFI has also been proposed [82]. The choice of correct model order is then crucial for performance.

Although shown to have potential for velocity estimation in CFI, these methods described have not been fully validated in-vivo, and are still considered experimental.

2.2.7 Blood flow parameter visualization

Arbitration

Before display, the parametric information in CFI is combined with the tissue B-mode image for duplex operation. For each image pixel, a decision is made whether tissue or flow information is to be displayed. This hard arbitration mechanism is a way to combine the two sources of information, but it is also necessary to reduce the amount of artifacts related to the limitations of the current CFI processing. The decision is typically based on comparisons of the power and frequency estimates of the Doppler signal. An example of arbitration rule could be that higher mean frequencies indicate blood signal, but simultaneously high power estimates may indicate flashing artifacts. For this image point the tissue image should be displayed. However, such simple threshold decisions are prone to error, and artifacts therefore occur.

Visualization

The visualization of the estimated blood flow velocity parameters is based on color encoding [30, 43]. The most basic visualization is to encode only the mean Doppler frequency magnitude and direction. In this one-dimensional color scheme, the axial direction of flow directed towards the away from the transducer is typically encoded in different colors, while the velocity magnitude is encoded in an increased color intensity. By further using a two-dimensional color scheme where the power estimates also control the intensity of the color, a better delineation of the vessel walls can be given. In cardiac imaging, it is common to use a two-dimensional colormap based on flow velocity and bandwidth. In this mode areas of high bandwidth indicating turbulence are highlighted in green color.

Another type of CFI visualization relies only on the Doppler signal power estimate and has been named power-Doppler [83, 84]. This method is often combined with a high degree of temporal averaging to produce angiography-like images suitable for imaging of smaller vessels and low flow rates in stationary tissue, such as in abdominal imaging.

Due to the spatial extents of the point spread function in ultrasound imaging, the tissue and flow information will inherently overlap when close to one another, and lead to color blooming artifacts where the flow image may cover areas of tissue. The immediate vessel wall can for instance often be covered by the color image. This problem is further aggravated when the spatial resolution for the flow image must be reduced in order to achieve a sufficient sensitivity.

2.3 Adaptive clutter rejection in CFI

2.3.1 Filter bank approach

One approach to adaptive clutter filtering has been to select an appropriate fixed-response clutter filter for each range gate based on estimated clutter Doppler signal characteristics, such as for instance the clutter mean velocity and power. A method for iteratively selecting the appropriate cut-off frequency of polynomial regression filters has been described [85], and a method for selecting the appropriate filter from a predefined set of high-pass filters has been proposed [86].

One drawback of these methods is the ad-hoc nature of optimizing the appropriate filters for different mixtures of clutter and blood signal. Further, since the methods depend on the estimated mean frequency of the clutter signal, errors will be induced when these estimates are inaccurate. This may for instance occur inside the vessel lumen of larger arteries, where the clutter and blood signal power may become comparable. This will lead to a bias in the estimate of the mean clutter Doppler frequency. Also, accelerated clutter movement will increase the bandwidth of the clutter Doppler signal, and may also be a source of bias and variance when estimating the mean frequency of the clutter signal.

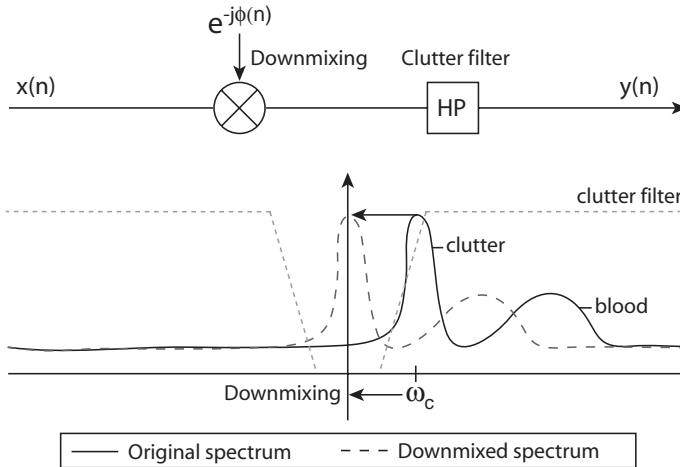


Figure 2.12: An illustration of the downmixing approach to adaptive clutter filtering. The received Doppler signal is downmixed using an estimate of the mean or varying clutter Doppler frequency.

2.3.2 Downmixing approach

Another adaptive filtering approach has been to process the received signal from each sample volume prior filtering. A Doppler signal downmixing technique was first proposed in [87, 88] for color flow imaging applications, and was given further elaboration in [89]. In this method, the complex slow-time Doppler signal is downmixed using a phase-function $\phi(n)$ based on estimates of the clutter Doppler frequency content, followed by a conventional non-adaptive high-pass filter. The concept is illustrated in Fig. 2.12. If successful, the clutter signal is moved to zero Doppler frequency, and a lower order clutter filter may then be used to remove the clutter component in varying conditions. This is beneficial for imaging both low and high velocities.

Estimates of the clutter Doppler frequency has been obtained using the autocorrelation approach as described in Section 2.2.6. The most simple technique performs downmixing using the estimates mean clutter Doppler frequency. The phase-function $\phi(n)$ used is then given by

$$\phi_{mf}(n) = \hat{\omega}_c n = \angle \left[\sum_{k=1}^{N_P-2} R_x(k, 1) \right] n \quad (2.37)$$

In this way adaptation to the tissue clutter velocity is achieved. This may be satisfactory when considering the relative movement between the transducer and patient. However, as rationalized in Section 2.2.4, the tissue movement also exhibits accelerated movement. The downmixing approach can be extended to adapt to acceleration by downmixing with a varying frequency obtained from the cumulative

phase of the correlation function of lag one. In this approach, the phase-function can be given by [89]

$$\phi_{vf}(n) = \begin{cases} 0 & \text{if } n = 0 \\ \sum_{k=1}^n \angle \hat{R}_x(k, 1) & \text{if } x = 1, \dots, N - 2 \end{cases} \quad (2.38)$$

To ensure the adaptation to the clutter signal, the autocorrelation estimates $\hat{R}_x(1)$ are averaged over a spatial region with similar characteristics.

As shown by Bjærum [89], the varying frequency approach is the most efficient of the two variants. However, the varying frequency approach must be used with caution as it may cause complications for subsequent velocity estimation. The mixing process with a varying frequency may cause artifacts in the resulting Doppler spectrum [90]. This does not occur for the constant mean frequency downmixing. A combined approach could be to use the varying frequency for power estimates, and the mean frequency downmixing for velocity estimates. By further doing arbitration based on the power estimates, flashing artifacts may be reduced. This has been proposed in a recent patent application by Germond-Rouet et al [90].

2.3.3 Eigenvector regression approach

A third approach to adaptive clutter rejection has been to design the clutter filter adaptively based on the received signal statistics. One such approach is eigenvector regression filtering. In this approach, the clutter signal is modeled as a linear combination of orthonormal basis vectors, obtained through the eigenvector decomposition of the signal correlation matrix. This approach to data representation and analysis has different origins and names, including principal component analysis (PCA), the Hotelling transform, and the (discrete) Karhunen-Loève transform (DKLT) [51]. Using the DKLT formulation, the received signal vector is expanded into the basis given by

$$\mathbf{x} = \sum_{i=1}^{N_P} \kappa_i \mathbf{e}_i, \quad E\{\kappa_i \kappa_j^*\} = \begin{cases} \lambda_i & i = j \\ 0 & i \neq j \end{cases} \quad (2.39)$$

where \mathbf{x} is a slow-time sample vector, and \mathbf{e}_i and λ_i are the eigenvectors and eigenvalues of the correlation matrix defined in (2.24). The expansion in (2.39) is sorted on decreasing eigenvalues λ_i , a measure of the variance or energy represented by an eigenvector \mathbf{e}_i . The DKLT follows when looking for an orthonormal basis expansion with statistically orthogonal expansion coefficients κ_i [51]. It can be shown that this is the most efficient representation of a random process in the mean-square sense, when the expansion is truncated to use fewer than N terms.

In the practical case, an estimated correlation matrix at a given point is obtained by averaging in a surrounding spatial region. The sample correlation matrix estimate is given by

$$\hat{\mathbf{R}}_x = \frac{1}{K} \sum_{k=1}^K \mathbf{x}_k \mathbf{x}_k^{*T}, \quad (2.40)$$

where K number of sample vectors that are used to form the estimate. The correlation matrix is in general Hermitian symmetric and positive semidefinite, and a complete (full rank) set of eigenvectors and orthonormal eigenvalues can be estimated if the number of independent sample vectors K in (4.19) is at least equal to the packet size N_P [91]. The eigenvectors then span the complete signal vector space. In the context of clutter filtering, a subset of these eigenvectors are selected for representing the clutter signal component, and removed through projection filtering. The final clutter filter can be formulated as a matrix-vector multiplication as for the polynomial regression filter, given by

$$y = \left(\mathbf{I} - \sum_{i=1}^M \hat{\mathbf{e}}_i \hat{\mathbf{e}}_i^{*T} \right) \mathbf{x} = \mathbf{A} \mathbf{x}, \quad (2.41)$$

where \mathbf{I} is the identity matrix and $\hat{\mathbf{e}}_i$ are the estimated eigenvectors selected for clutter representation. The filter order is defined as $M - 1$, i.e., a zero order filter includes one eigenvector. As the method relies on estimation of the correlation matrix based on spatial averaging of signal vectors, the eigenvectors will represent signal components based on the average of the estimated signal statistics. Uniform statistics is therefore assumed in the averaging region. When few sample vectors are used in the averaging process, the variance of the correlation matrix estimate might also be a source of error in clutter representation.

The question remains as to how to select the proper eigenvectors for clutter representation. This aspect is crucial for the success of the algorithm. If the chosen basis does not represent most of the clutter signal, it may not be properly attenuated, and a bias in subsequent velocity estimation is inferred. Further, if eigenvectors also representing the blood signal component is included, a substantial part of the blood signal may be lost. The information available for selection of the proper basis is given by the eigenvalues and eigenvectors. The eigenvalues has information about the signal energy or variance represented by the eigenvector basis vector. A dominant signal component that constitute a large part of the total signal variance, will therefore be represented by eigenvectors with large corresponding eigenvalues. Due to the dominant and low-bandwidth nature of the clutter Doppler signal, the clutter signal energy is mostly contained in the signal subspace represented by a smaller set of eigenvectors with large corresponding eigenvalues [89]. This has been the criteria used in prior investigations [89, 92], where a fixed number of eigenvector basis has been selected from the N_P eigenvectors with the most dominant eigenvalues. This method follows the truncated DKLT formulation. Among alternative basis representations used for clutter filtering, such as the Legendre polynomial basis, it is optimal in removing the most of the clutter signal for a given filter order. The approach assumes that the blood signal energy is low compared to that of clutter signal. As the mixture of clutter and blood signal varies throughout an image region, the appropriate filter order also varies, and should be chosen adaptively. The filter order can be selected based on the eigenvalue spectrum information, for instance by adaptive thresholding of the eigenvalue spectrum or the eigenvalue spectrum slope.

As an alternative or extension to this approach, one can also conceive estimating the frequency content of the individual eigenvectors, and base a decision on the fact

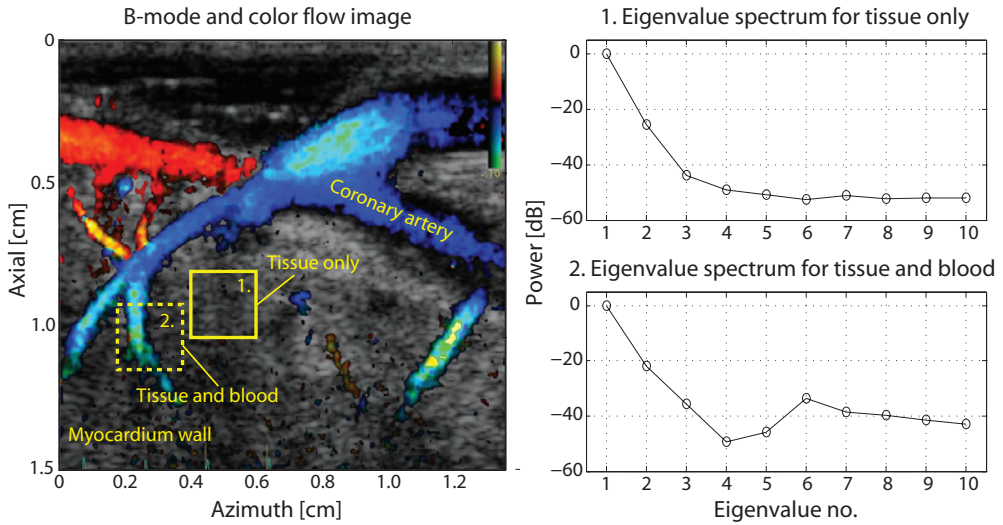


Figure 2.13: The eigenvalue spectrum from a region containing tissue signal only, and a region containing both tissue clutter and blood signal. The spectrum is sorted on increasing frequency content of the eigenvectors. As can be seen, when blood signal is introduced, it is represented by a different set of eigenvectors than that of tissue signal. The data was acquired from a beating pig myocardium using an i13L linear array (GE Healthcare, WI, USA) with a pulse center frequency of 10 MHz.

that the clutter signal typically has a lower frequency content than the signal from blood. The mean frequency of each eigenvector can for instance be estimated using the autocorrelation approach as described in Section 2.2.6. Aspects of both filter order selection schemes can be observed in Fig. 2.13. The example is based on data obtained from the beating heart of a pig, using an i13L linear array (GE Healthcare, WI, USA) with a pulse center frequency of 10 MHz. The eigenvalues have been sorted on the estimated mean frequency of each eigenvector. The clutter signal is in this example mostly represented by the first three eigenvectors. The blood signal is mostly represented by a different part of the spectrum with a higher frequency content. As can be observed by careful inspection of this example, using only the signal energy as a criteria for selecting eigenvectors would also have removed a substantial part of the blood signal if the three most dominating eigenvectors had been chosen.

An advantage of the eigenvector regression approach compared to conventional clutter filters is the fact that it can adapt to non-stationary movement. As described in Section 2.2.4, the tissue clutter signal is typically accelerated, and the received clutter signal thus exhibits this non-stationary behavior. The potential performance gain obtained from this property in a practical setting remains to be investigated.

2.3.4 Independent component analysis

Some efforts have been made to analyze and remove the clutter signal component by independent component analysis (ICA) [93, 94], based on the JADE algorithm described by Cardoso [95]. This is a blind signal separation approach based on the non-Gaussian characteristics of the signal components of interest. In the case of CFI, the Gaussian assumption for the blood signal component is well rationalized. For the tissue component, the different scattering characteristics throughout an image region may lead to an averaged non-Gaussian distribution. As the estimation of statistics for the signal components must be based on the assumption of uniform statistics in a region of interest, small averaging regions must be employed. As discussed in Section 2.2.4, the distribution of the tissue signal then typically approaches a Gaussian shape. Using ICA and higher-order statistics are therefore not expected to give an increase in performance compared to using a second-order Gaussian approach. The methods are therefore not properly justified for the task of clutter rejection.

2.4 Vector velocity imaging in CFI

2.4.1 Compound Doppler and related techniques

Compound Doppler approach

By utilizing several Doppler measurements from different beam angles, an estimate of the blood flow velocity vector can be obtained. This compound Doppler approach has been a area of research in over 30 years, and an excellent review for both PW-Doppler and CFI systems is given by Dunmire [96]. Two main approaches have been used for compound Doppler in CFI. Either combining two or three regular CFI acquisitions steered in different directions [97], or to simultaneously use separate subapertures on the same transducer array for transmit and receive [98–100]. For use in CFI the most practical approach is to transmit in one direction, and to receive and beamform from two directions in parallel using separate subapertures. This particular setup is illustrated in Fig. 2.14. In this way using parallel receive beamforming, only one frame acquisition is needed, critical for following the dynamics of the flow. The axial and lateral velocity component in this two-dimensional setup is then given by [96]

$$v_{lat} = \frac{c \cdot (f_l - f_r)}{2f_0 \cdot \sin \theta}, \quad v_{ax} = \frac{c \cdot (f_l + f_r)}{2f_0 \cdot (1 + \cos \theta)}, \quad (2.42)$$

where f_l and f_r is the Doppler shift received from the left and right subaperture respectively, and θ is the angle between the receive and transmit directions. This angle can be kept constant in depth by beam steering and by gradually sliding the receive subapertures from the middle towards the ends of the transducer for increasing depths.

Limitations of the compound Doppler approach is mainly related to the problem of achieving a sufficient angle of separation between the beam directions to obtain a sufficient accuracy in velocity measurements for increasing depths. Also, for transducer

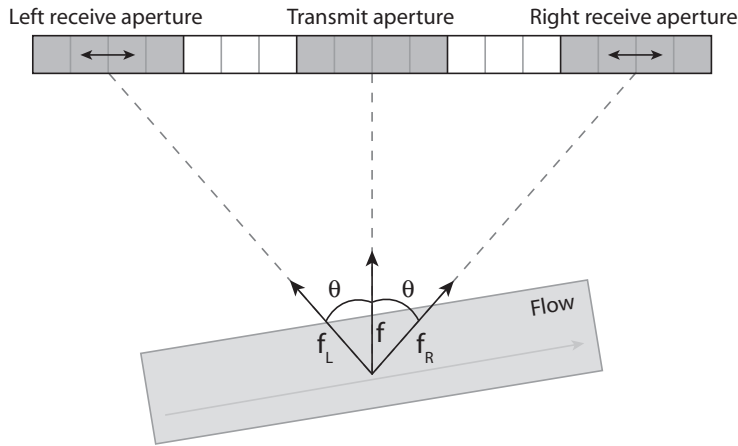


Figure 2.14: A compound Doppler approach for CFI utilizing one transmit aperture and two receive apertures beamformed in parallel.

subarray approaches, the receive apertures will be reduced in size, compromising the sensitivity. Although the compound Doppler approach has been validated to give reasonable accurate results in different vascular contexts, no mainstream system is available, and clinical studies rationalizing the use of the method are still limited [96].

Lateral modulation approach

Another approach related to the compound Doppler technique has been proposed by Jensen and Munk [101] and Anderson [102]. The methods are based on producing a modulation in the lateral direction of the received ultrasound field, using complex apodization schemes. A scatterer movement in the lateral direction can then be registered using a phase-shift technique as in the radial direction.

The approach taken by Anderson has been called spatial quadrature, and relies on the use of a complex apodization scheme on receive to create the lateral modulation. Using odd and even apodization functions related by a Hilbert operator, an in-phase and quadrature PSF can be produced using parallel beamforming on receive. The two different receive signals are added and subtracted to produce a signal from a left and right receive subaperture, respectively, as defined by the distance between the peaks of the apodization functions.

The approach by Jensen and Munk has been named transverse oscillation. Two sinc-shaped receive apertures placed a distance apart have been used to create the lateral modulation on receive. To have a spatial modulation that only depends on the receive field, a near uniform beam is transmitted using a Gaussian transmit apodization. The in-phase and quadrature signal from the lateral modulation is directly sampled by steering two receive beams one quarter of a wavelength apart symmetrically around the transmit beam direction. This can be done by parallel beamforming in one frame acquisition.

In both methods the lateral modulation is approximated to be given through the Fraunhofer approximation as the Fourier transform of two point sources placed a distance apart. This results in a sinusoidal modulation given by

$$r_{lat}(t) = \cos\left(2\pi\frac{D}{z\lambda}t\right) = \cos(2\pi f_{lat}t), \quad (2.43)$$

where D is the distance between the two point sources, z is the depth of interest, and λ is the wavelength of the emitted pulse.

Compared to the compound Doppler approach described above, the lateral modulation approaches uses complex apodization schemes to obtain the signal from two separated subapertures on receive. Using a Hilbert transform as in the spatial quadrature approach, is in theory identical to the compound Doppler method described. This relation was also indicated by Anderson [103]. The transverse oscillation method on the other hand, uses a narrowband approximation to the Hilbert transform, and this method is therefore at best equal to the other two.

2.4.2 Doppler bandwidth method

The bandwidth of the received composite Doppler signal is dependent on the spread of velocities of the scatterers present. It is further also dependent on the finite observation time of individual scatterers given as they travel through the sample volume [104, 105]. This is termed the transit-time broadening effect. Several authors have proposed models of the Doppler bandwidth variation [106–108], and the idea of estimating the lateral flow component based on the estimated Doppler bandwidth [109–111]. To obtain a bandwidth dependency independent of different beam-to-vessel angles, the methods has been based on shaping the Doppler sample volume spherically [107]. As non-stationary behavior will also contribute to the doppler spectral bandwidth, the methods are based on stationary flow assumptions.

The main challenge of this method is perhaps to obtain a robust estimate of the true Doppler signal bandwidth in a realistic setting. This can be in general be problematic in low signal-to-noise conditions. The clutter signal will also be a problem if not properly removed. This could especially be problematic in the systole part of the cardiac cycle at the time of the incoming flow pulse. The clutter rejection filter will further cause problems when the flow direction approaches a transverse direction compared to the beam, as a major part of the Doppler signal from blood may then be removed. These confounding factors has kept the Doppler bandwidth method at an experimental stage.

2.4.3 Speckle tracking techniques

The lateral velocity components of blood will move the blood scatterers out of the axial beam direction. As an extension to the 1-D axial cross-correlation technique, one can conceive searching for the maximum signal correlation between image acquisitions in the two-dimensional image plane, or even the three-dimensional image volume. The velocity vector can then be in principle measured based on the distance to the point of

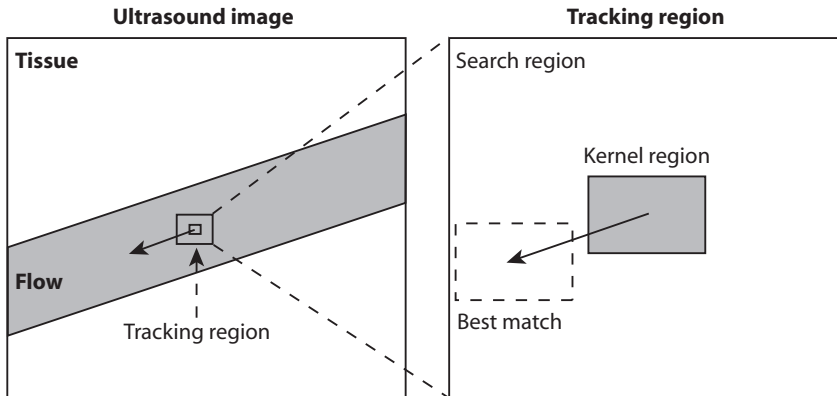


Figure 2.15: An illustration of the speckle tracking concept. The best match of a given kernel region is searched for in a larger search area of a subsequent acquisition. The velocity can be calculated based on the estimated displacement and the time between image acquisitions.

maximum correlation and the time between image acquisitions. Due to computational demands of two- or three-dimensional cross-correlation, this is difficult to do in real-time at present. However, methods have been proposed that approximate the true correlation function with similar measures. To further reduce the complexity, the methods also operate on the signal envelope rather than the RF-signal. By matching speckle pattern regions in subsequent frames an estimate of the displacement and velocity of the given pattern is given by the position of the best match. This concept, referred to as speckle tracking, is shown in Fig. 2.15 for the two-dimensional case.

Common correlation measures include the sum of absolute differences (SAD), or the sum of squared differences (SSD) of image patterns. Considering X_0 as the kernel region and X_1 to be region in a search area in a subsequent image acquisition, the SAD formula can be written as [112]:

$$\epsilon(\alpha, \beta) = \sum_{k=1}^K \sum_{l=1}^L |X_0(k, l) - X_1(k - \alpha, l - \beta)|, \quad (2.44)$$

where the quantity ϵ is termed the SAD coefficient, K and L defines the lateral and axial size of the kernel region, and α and β defines the offset compared to the center in the search region. Pushed by the demands of multimedia video compression, SAD calculations are now an integral part of the multimedia instruction sets on modern CPUs [113], which can substantially increase the efficiency of an SAD tracking implementation.

The concept of ultrasound speckle tracking for flow velocity vector estimation was proposed at Duke University [114, 115]. This group also developed a system capable of producing approximately 800 velocity vector estimates in real-time [116], which was analyzed in-vitro and in-vivo in a series of papers [117, 118]. Their efforts were

summarized in [112]. In general, a good correlation in velocity vector estimates was reported for regular lateral flow and high signal-to-noise ratios. Axial flow components severely decreased the accuracy of the method. Clinical in-vivo studies have not been performed.

The main limitations of the speckle tracking approach for blood flow velocity vector estimation are related to clutter filtering and speckle pattern decorrelation. To achieve a sufficient attenuation of the clutter signal while retaining the signal from blood, the imaging frame rate of the two- or three-dimensional search region must be high compared to the Doppler shifts produced by the movement of tissue. Also, when the direction of flow approaches a pure lateral direction, the Doppler shifts approaches zero, and a large part of the blood signal will be removed using traditional clutter rejection filters. Due to the lateral bandwidth of the imaging system, some blood signal will typically remain after filtering. As shown in [122], a bandpass signal is then produced, inferring an amplitude modulation in the remaining speckle pattern.

The blood flow speckle pattern rapidly decorrelates due to sources such as non-laminar flow patterns, flow velocity gradients, and out-of-plane movement in two-dimensional velocity estimation. This speckle decorrelation can severely degrade the performance of the speckle tracking procedure. Due to the bandpass nature and higher spatial frequency content in the axial direction, the decorrelation is more prominent when a substantial axial velocity component is present [119].

The high imaging frame rate of lateral subregions needed may be obtained by using beam interleaving techniques as described in Section 2.2.3. Smaller subimages are then obtained at a frame rate equal to the pulse repetition frequency. As there is no correlation of the speckle pattern between interleave groups, the speckle tracking algorithm must be performed within one group. Also, as the interleave group width shrink for increasing scan depths, so will the width of the search regions. Another approach is to track the speckle signal within groups of receive lines acquired using multiple line acquisition (MLA) [120, 121]. In this way, very small subregions can be acquired simultaneously at a very high frame rate. Two or four times MLA is today common in high-end scanners, but this is will be further increased due to the demands of frame rate imposed by dynamic three-dimensional imaging.

Another challenge in speckle tracking is related to spatial sampling and interpolation. The movement of scatterers as estimated using speckle tracking is limited to a displacement of an integer number of beam and range samples. To ensure a sufficient overall frame rate for following the flow dynamics, the lateral sampling is limited, and interpolation methods then becomes crucial in order to estimate the movement of the scatterers with good accuracy.

In summary, although efforts have shown that speckle tracking of blood is feasible, the lack of robustness for irregular flow patterns and the challenge of clutter filtering has kept the method at an experimental stage.

2.5 Future directions of CFI systems

Future CFI systems has more to offer. Current trends of real-time 3-D ultrasound imaging is at the moment pushing the technology forward, and also offer new possibilities for improved 2-D imaging. Transducer, transmitter, and beamforming technology is becoming increasingly more sophisticated, and the continuing increase in computational power of standard CPUs and graphic card GPUs, opens up for the use of more advanced real-time signal processing that can be more easily implemented and evaluated.

An improved separation of flow through adaptive signal processing can be expected to improve the estimation of low-velocity flow in peripheral vessels, and to provide a better image of coronary flow in transthoracic imaging. High-frequency imaging of the microcirculation such as for the detection of angiogenesis in cancer diagnosis might also be possible in combination with more advanced clutter rejection in the future.

High-frequency imaging in the 20-80 MHz range has for practical purposes conventionally been done using mechanically steered transducers, and the CFI performance is then more challenging then for transducer arrays [123]. Current research efforts are however producing increasingly robust high-frequency arrays [124], which may increase the performance of high-frequency microcirculation imaging.

Real-time dynamic three-dimensional color flow imaging is now available, and is expected to increase the certainty of diagnosis of cardiac abnormalities such as the quantification of valve leakage area. One of the challenges of this modality is to achieve a sufficient frame rate. Currently, ECG triggering over several heart cycles is needed to obtain a sufficiently large imaging volume sector at tolerable frame rates. An increased frame rate can be expected by the use of more parallel receive beamforming, however, the number of parallel receive beams is ultimately limited by demands of penetration, as the transmit beam must be broad enough to cover all receive beams. Adaptive clutter rejection techniques may further be used to lower the packet size in CFI to achieve a higher frame rate [90].

Two- and three-dimensional vector velocity estimation has been a continuing area of research. At the moment, compound Doppler techniques and speckle tracking are perhaps the most liable candidates for accomplishing this task in the near future. Real-time operation of both these methods is today considered feasible. In high-frequency flow imaging the use of speckle tracking becomes more attractive as the signal power of blood then becomes comparable to that of tissue, and can then be tracked with less demands of clutter filtering [125].

References

- [1] J. Wild and J. Reid, "Application of echo-ranging techniques to the determination of structure of biological tissues," *Science*, vol. 115, pp. 226–230, 1952.
- [2] D. Howry and W. Bliss, "Ultrasonic visualization of soft tissue structures of the body," *J. Lab. Clin. Med.*, vol. 40, pp. 579–592, 1952.
- [3] I. Edler and C. Hertz, "The use of ultrasonic reflectoscope for the continuous recording of the movements of heart walls. 1954," *Clin Physiol Funct Imaging*, vol. 24, pp. 118–136, 2004.
- [4] P. Wells, "Ultrasound imaging," *Phys. Med. Biol.*, vol. 51, pp. R83–R98, 2006.
- [5] K. Taylor and P. Wells, "Tissue characterisation," *Ultrasound Med. Biol.*, vol. 15, pp. 421–428, 1989.
- [6] J. Somer, "Electronic sector scanning for ultrasonic diagnosis," *Ultrasonics*, vol. 6, pp. 153–159, 1968.
- [7] J. Griffith and W. Henry, "A sector scanner for real time two-dimensional echocardiography," *Circulation*, vol. 49, pp. 1147–1152, 1974.
- [8] O. Ramm and F. Thurstone, "Cardiac imaging using a phased array ultrasound system. i. system design," *Circulation*, vol. 53, pp. 258–262, 1976.
- [9] S. Satomura, "Ultrasonic doppler method for the inspection of cardiac functions," *J. Acoust. Soc. Am.*, vol. 29, pp. 1181–1185, 1957.
- [10] P. Peronneau and F. Leger, "Doppler ultrasonic pulsed blood flowmeter," *Proc. 8th Int. Conf. Med. Biol. Eng.*, pp. 10–11, 1969.
- [11] P. Wells, "A range-gated ultrasonic doppler system," *Med. Biol. Eng.*, vol. 7, pp. 641–652, 1969.
- [12] D. Baker, "Pulsed ultrasonic doppler blood-flow sensing," *IEEE Trans. Sonics Ultrason.*, vol. 17, pp. 170–185, 1970.

-
- [13] B. Goldberg, R. Gramiak, and A. Freimanis, "Early history of diagnostic ultrasound: the role of american radiologists," *AJR. Am. J. Roentgenol.*, vol. 160, pp. 189–194, 1993.
- [14] K. Beach, "1975-2000: a quarter century of ultrasound technology," *Ultrasound Med. Biol.*, vol. 18, pp. 377–388, 1992.
- [15] P. Callen, *Ultrasonography in obstetrics and gynecology, 4th edition*. Philadelphia: Elsevier/Saunders Publishing Company, 2000.
- [16] A. Weyman, *Principles and Practice of Echocardiography*. Philadelphia: Lippincott Williams & Wilkins, 1993.
- [17] M. Hennerici, D. Neuerburg-Heusler, M. Daffertshofer, T. Karasch, and S. Meairs, *Vascular Diagnosis With Ultrasound: Clinical References With Case Studies, 2nd edition*. New York: Thieme Medical Publishers, 2006.
- [18] C. Rumack, S. Wilson, and J. Charboneau, *Diagnostic ultrasound*. St. Louis: Elsevier Mosby, 2005.
- [19] H. Feigenbaum, W. Armstrong, and T. Ryan, *Feigenbaum's echocardiography, 6th edition*. Philadelphia: Lippincott Williams & Wilkins, 2005.
- [20] W. McDicken, *Diagnostic ultrasonics: principles and use of instruments*. Edinburgh: Churchill Livingstone, 1991.
- [21] D. Evans and W. McDicken, *Doppler ultrasound: physics, instrumentation and clinical applications, 2nd edition*. Chichester: John Wiley & Sons, 2000.
- [22] B. Angelsen, *Ultrasound imaging: waves, signals, and signal processing*. Trondheim: Emantec AS, 2000.
- [23] G. Ludwig, "The velocity of sound through tissues and the acoustic impedance of tissues," *J. Acoust. Soc. Am.*, vol. 22, pp. 862–866, 1950.
- [24] F. Duck, *Physical properties of tissue: a comprehensive reference book*. London: Academic Press, 1990.
- [25] R. Lerner and R. Waag, "Wave space interpretation of scattered ultrasound," *Ultrasound Med. Biol.*, vol. 14, pp. 97–102, 1988.
- [26] A. Roguin, "Christian johann doppler: the man behind the effect," *Br. J. Radiol.*, vol. 75, pp. 615–619, 2002.
- [27] J. Jensen, *Estimation of Blood Velocities Using Ultrasound - A Signal Processing Approach*. New York: Cambridge University Press, 1996.
- [28] P. Atkinson and J. Woodcock, *Doppler ultrasound and its use in clinical measurement*. London: Academic Press, 1982.

- [29] M. Brandestini, "Topoflow-a digital full range doppler velocity meter," *IEEE Trans. Sonics Ultrason.*, vol. 25, pp. 287–292, 1978.
- [30] M. Eyer, M. Brandestini, D. Phillips, and D. Baker, "Color digital echo/doppler image presentation," *Ultrasound Med. Biol.*, vol. 7, pp. 21–31, 1981.
- [31] J. Reid and M. Spencer, "Ultrasonic doppler technique for imaging blood vessels," *Science*, vol. 176, pp. 1235–1236, 1972.
- [32] K. Kristoffersen and B. Angelsen, "A comparison between mean frequency estimators for multigated doppler systems with serial signal processing," *IEEE Trans. Biomed. Eng.*, vol. 32, pp. 645–657, 1985.
- [33] B. Angelsen and K. Kristoffersen, "Discrete time estimation of the mean doppler frequency in ultrasonic blood velocity measurements," *IEEE Trans. Biomed. Eng.*, vol. 30, pp. 207–214, 1983.
- [34] W. Barber, J. Eberhard, and S. Karr, "A new time domain technique for velocity measurements using doppler ultrasound," *IEEE Trans. Biomed. Eng.*, vol. 32, pp. 213–229, 1985.
- [35] K. Kristoffersen, "Time-domain estimation of the center frequency and spread of doppler spectra in diagnostic ultrasound," *IEEE Trans. Ultrason., Ferroelec., Freq. Contr.*, vol. 35, pp. 484–497, 1988.
- [36] C. Kasai, K. Namekawa, A. Koyano, and R. Omoto, "Real-time two-dimensional blood flow imaging using an autocorrelation technique," *IEEE Trans. Sonics Ultrason.*, vol. 32, pp. 458–464, 1985.
- [37] K. Namekawa, C. Kasai, M. Tsukamoto, and A. Koyano, "Realtime bloodflow imaging system utilizing auto-correlation techniques," *Ultrasound Med. Biol.*, vol. Suppl 2, pp. 203–208, 1983.
- [38] K. Miller and M. Rochwarger, "A covariance approach to spectral moment estimation," *IEEE Trans. Informat. Theor.*, vol. 18, pp. 588–596, 1972.
- [39] D. Sirmans and B. Bumgarner, "Numerical comparison of five mean frequency estimators," *J. Appl. Meteorol.*, vol. 14, pp. 991–1003, 1975.
- [40] D. Zrnic, "Spectral moment estimates from correlated pulsed pair," *IEEE Trans. Aerosp. Electron.*, vol. 13, pp. 344–354, 1977.
- [41] G. Gray, R. Serafin, D. Atlas, R. Rineheart, and J. Boyajian, "Real-time color doppler radar display," *American Meteorological Society Bulletin*, vol. 56, pp. 580–588, 1975.
- [42] H. Torp and B. Angelsen, *Estimation of blood velocities from Doppler signals. Ultrasound imaging, Waves, Signals, and Signal Processing vol. 2*. Trondheim: Emantec AS, 2000.

-
- [43] P. Wells, "Ultrasonic colour flow imaging," *Phys. Med. Biol.*, vol. 39, pp. 2113–2145, 1994.
- [44] K. Ferrara and G. DeAngelis, "Color flow mapping," *Ultrasound in Medicine & Biology*, vol. 23, pp. 321–345, 1997.
- [45] K. Kristoffersen, "Optimal receiver filtering in pulsed doppler ultrasound blood velocity measurements," *IEEE Trans. Ultrason., Ferroelec., Freq. Contr.*, vol. 33, pp. 51–58, 1986.
- [46] B. Haider, P. Lewin, and K. Thomenius, "Pulse elongation and deconvolution filtering for medical ultrasonic imaging," *IEEE Trans. Ultrason., Ferroelect., Freq. Contr.*, vol. 45, pp. 98–113, 1998.
- [47] T. Misaridis, K. Gammelmark, C. Jorgensen, N. Lindberg, A. Thomsen, M. Pedersen, and J. Jensen, "Potential of coded excitation in medical ultrasound imaging," *Ultrasonics*, vol. 38, pp. 183–189, 2000.
- [48] D. Shattuck, M. Weinshenker, S. Smith, and O. Ramm, "Explososcan: A parallel processing technique for high speed ultrasound imaging with linear phased arrays," *J. Acoust. Soc. Am.*, vol. 75, pp. 1273–1282, 1984.
- [49] K. Thomenius, "Evolution of ultrasound beamformers," *Proceedings of the IEEE Ultrasonics Symposium, 1996*, vol. 2, pp. 1615–1622 vol2, 1996.
- [50] R. Chesarek, "Ultrasound imaging system for relatively low-velocity blood flow at relatively high frame rates," *US Patent 4888694, Quantum Medical Systems, Inc.*, 1989.
- [51] C. Therrien, *Discrete Random Signals and Statistical Signal Processing*. Prentice Hall Inc., 1992.
- [52] B. Angelsen, "A theoretical study of the scattering of ultrasound from blood," *IEEE Trans. Biomed. Eng.*, vol. BME-27, pp. 61–67, 1980.
- [53] R. Albright, "Relationship of doppler ultrasonic scattered signal characteristics to flow and beam parameters," *The Journal of the Acoustical Society of America*, vol. 59, pp. 786–789, 1976.
- [54] L. Mo and R. Cobbold, "A stochastic model of the backscattered doppler ultrasound from blood," *IEEE Trans. Biomed. Eng.*, vol. 33, pp. 20–27, 1986.
- [55] P. Atkinson and M. Berry, "Random noise in ultrasonic echoes diffracted by blood," *Journal of Physics A: Mathematical, Nuclear and General*, vol. 7, pp. 1293–1302, 1974.
- [56] K. Shung, G. Cloutier, and C. Lim, "The effects of hematocrit, shear rate, and turbulence on ultrasonic doppler spectrum from blood," *IEEE Trans. Biomed. Eng.*, vol. 39, pp. 462–469, 1992.

- [57] S. Wang and K. Shung, "In vivo measurements of ultrasonic backscattering in blood," *IEEE Trans. Ultrason., Ferroelect., Freq. Contr.*, vol. 48, pp. 425–431, 2001.
- [58] L. Mo and R. Cobbold, "A unified approach to modeling the backscattered doppler ultrasound from blood," *IEEE Trans. Biomed. Eng.*, vol. 39, pp. 450–461, 1992.
- [59] H. Torp, K. Kristoffersen, and B. Angelsen, "Autocorrelation technique in color flow imaging, signal model and statistical properties of the autocorrelation estimates," *IEEE Trans. Ultrason., Ferroelec., Freq. Contr.*, vol. 41, pp. 604–612, 1994.
- [60] M. Aygen and R. Popp, "Influence of the orientation of myocardial fibers on echocardiographic images," *Am. J. Cardiol.*, vol. 60, pp. 147–152, 1987.
- [61] R. Wagner, S. Smith, J. Sandrik, and H. Lopez, "Statistics of speckle in ultrasound b-scans," *IEEE Trans. Sonics Ultrason.*, vol. 30, pp. 156–163, 1983.
- [62] A. Heimdal and H. Torp, "Ultrasound doppler measurements of low velocity blood flow: limitations due to clutter signals from vibrating muscles," *Ultrasonics, Ferroelectrics and Frequency Control, IEEE Transactions on*, vol. 44, pp. 873–881, 1997.
- [63] H. Torp, "Clutter rejection filters in color flow imaging: A theoretical approach," *IEEE Trans. Ultrason., Ferroelec., Freq. Contr.*, vol. 44, pp. 417–424, 1997.
- [64] S. Bjaerum, H. Torp, and K. Kristoffersen, "Clutter filter design for ultrasound color flow imaging," *IEEE Trans. Ultrason., Ferroelec., Freq. Contr.*, vol. 49, pp. 204–216, 2002.
- [65] A. Hoeks, J. Vandevorst, A. Dabekaussen, P. Brands, and R. Reneman, "An efficient algorithm to remove low-frequency doppler signals in digital doppler systems," *Ultrason. Imaging*, vol. 13, pp. 135–144, 1991.
- [66] A. Kadi and T. Loupas, "On the performance of regression and step-initialized iir clutter filters for color doppler systems in diagnostic medical ultrasound," *IEEE Trans. Ultrason., Ferroelec., Freq. Contr.*, vol. 42, pp. 927–937, 1995.
- [67] R. Fletcher and D. Burlage, "Initialization technique for improved mti performance in phased-array radars," *Proceed. IEEE*, vol. 60, pp. 1551–1552, 1972.
- [68] E. Chornoboy, "Initialization for improved iir filter performance," *IEEE Trans. Signal Process.*, vol. 40, pp. 543–550, 1992.
- [69] J. Willemetz, A. Nowicki, J. Meister, F. D. Palma, and G. Pante, "Bias and variance in the estimate of the doppler frequency induced by a wall motion filter," *Ultrason. Imaging*, vol. 11, pp. 215–225, 1989.

-
- [70] J. Rajaonah, B. Dousse, and J. Meister, "Compensation of the bias caused by the wall filter on the mean doppler frequency," *IEEE Trans. Ultrason., Ferroelec., Freq. Contr.*, vol. 41, pp. 812–819, 1994.
- [71] R. Doviak and D. Zrnic, "Practical algorithms for mean velocity estimation in pulse doppler weather radars using a small number of samples," *IEEE Trans. Geosci. Remote Sensing*, vol. 21, pp. 491–501, 1983.
- [72] H. Torp, K. Kristoffersen, and A. Angelsen, "On the joint probability density function for the autocorrelation estimates in ultrasound color flow imaging," *IEEE Trans. Ultrason., Ferroelec., Freq. Contr.*, vol. 42, pp. 899–906, 1995.
- [73] T. Loupas, J. Powers, and R. Gill, "An axial velocity estimator for ultrasound blood flow imaging, based on a full evaluation of the doppler equation by means of a two-dimensional autocorrelation approach," *Ultrasonics, Ferroelectrics and Frequency Control, IEEE Transactions on*, vol. 42, pp. 672–688, 1995.
- [74] O. Bonnefous and P. Pesque, "Time domain formulation of pulse-doppler ultrasound and blood velocity estimation by cross correlation," *Ultrason. Imaging*, vol. 8, pp. 73–85, 1986.
- [75] S. Foster, P. Embree, and W. O'Brien, "Flow velocity profile via time-domain correlation: error analysis and computer simulation," *Ultrasonics, Ferroelectrics and Frequency Control, IEEE Transactions on*, vol. 37, pp. 164–175, 1990.
- [76] P. Embree and W. O'Brien, "The accurate ultrasonic measurement of the volume flow of blood by time domain correlation," *Ultrasonics Symposium, IEEE 1985*, pp. 963–966, 1985.
- [77] H. Torp, X. Lai, and K. Kristoffersen, "Comparison between cross-correlation and auto-correlation technique in color flow imaging," *Ultrasonics Symposium, 1993 Proceedings, IEEE 1993*, pp. 1039–1042 vol2, 1993.
- [78] K. Ferrara and V. Algazi, "A new wideband spread target maximum likelihood estimator for blood velocity estimation. i. theory," *IEEE Trans. Ultrason., Ferroelec., Freq. Contr.*, vol. 38, pp. 1–16, 1991.
- [79] L. Wilson, "Description of broad-band pulsed doppler ultrasound processing using the two-dimensional fourier transform," *Ultrason. Imaging*, vol. 13, pp. 301–315, 1991.
- [80] S. Alam and K. Parker, "The butterfly search technique for estimation of blood velocity," *Ultrasound in Medicine & Biology*, vol. 21, pp. 657–670, 1995.
- [81] P. Vaitkus and R. Cobbold, "A new time-domain narrowband velocity estimation technique for doppler ultrasound flow imaging. i. theory," *IEEE Trans. Ultrason., Ferroelec., Freq. Contr.*, vol. 45, pp. 939–954, 1998.

- [82] Y. Ahn and S. Park, "Estimation of mean frequency and variance of ultrasonic doppler signal by using second-order autoregressive model," *IEEE Trans. Ultrason., Ferroelec., Freq. Contr.*, vol. 38, pp. 172–182, 1991.
- [83] S. Jain, P. Fan, E. Philpot, N. Nanda, K. Aggarwal, S. Moos, and A. Yoganathan, "Influence of various instrument settings on the flow information derived from the power mode," *Ultrasound Med. Biol.*, vol. 17, pp. 49–54, 1991.
- [84] J. Rubin, R. Bude, P. Carson, R. Bree, and R. Adler, "Power doppler us: a potentially useful alternative to mean frequency-based color doppler us," *Radiology*, vol. 190, pp. 853–856, 1994.
- [85] S. Bjærum, H. Torp, T. Bakke, and K. Kristoffersen, *Detection and visualization of moving targets in medical ultrasound imaging, paper E: Automatic selection of the clutter filter cut-off frequency in ultrasound color flow imaging*, pp. E1–E14. Trondheim, Norway: Norwegian University of Science and Technology, 2001.
- [86] Y. Yoo, R. Managuli, and Y. Kim, "Adaptive clutter filtering for ultrasound color flow imaging," *Ultrasound Med. Biol.*, vol. 29, pp. 1311–1320, 2003.
- [87] L. Thomas and A. Hall, "An improved wall filter for flow imaging of low velocity flow," *Proceedings of the IEEE Ultrasonics Symposium*, vol. 3, pp. 1701–1704, 1994.
- [88] P. Brands, A. Hoeks, and R. Reneman, "The effect of echo suppression on the mean velocity estimation range of the rf cross-correlation model estimator," *Ultrasound Med. Biol.*, vol. 21, pp. 945–959, 1995.
- [89] S. Bjaerum, H. Torp, and K. Kristoffersen, "Clutter filters adapted to tissue motion in ultrasound color flow imaging," *IEEE Trans. Ultrason., Ferroelec., Freq. Contr.*, vol. 49, pp. 693–704, 2002.
- [90] L. Germond-Rouet, L. Thanasis, and O. Bonnefous, "Clutter filtering with small ensemble lengths in ultrasound imaging," *International Patent no. WO 2005/033737 A1, Philips Electronics N.V.*, 2005.
- [91] G. Golub and C. V. Loan, *Matrix Computations*. Johns Hopkins University Press, 1996.
- [92] D. Kruse and K. Ferrara, "A new high resolution color flow system using an eigendecomposition-based adaptive filter for clutter rejection," *IEEE Trans. Ultrason., Ferroelect., Freq. Contr.*, vol. 49, pp. 1384–1399, 2002.
- [93] C. Gallippi and G. Trahey, "Adaptive clutter filtering via blind source separation for two-dimensional ultrasonic blood velocity measurement," *Ultrason. Imaging*, vol. 24, pp. 193–214, 2002.
- [94] C. Gallippi, K. Nightingale, and G. Trahey, "Bss-based filtering of physiological and arfi-induced tissue and blood motion," *Ultrasound Med. Biol.*, vol. 29, pp. 1583–1592, 2003.

-
- [95] J. Cardoso and A. Souloumiac, "Blind beamforming for non-gaussian signals," *Radar and Signal Processing, IEE Proceedings F*, vol. 140, pp. 362–370, 1993.
- [96] B. Dunmire, K. Beach, K. Labs, M. Plett, and D. Strandness, "Cross-beam vector doppler ultrasound for angle-independent velocity measurements," *Ultrasound Med. Biol.*, vol. 26, pp. 1213–1235, 2000.
- [97] D. Fei, C. Fu, W. Brewer, and K. Kraft, "Angle independent doppler color imaging: Determination of accuracy and a method of display," *Ultrasound in Medicine & Biology*, vol. 20, pp. 147–155, 1994.
- [98] E. Papadofrangakis, W. Engeler, and J. Fakiris, "Measurement of true blood velocity by an ultrasound system," *US Patent no. 4,265,126, General Electric Company*, 1981.
- [99] A. Hall and R. Bernandi, "Method for detecting two-dimensional flow for ultrasound color flow imaging," *US Patent No. 5,398,216, General Electric Company*, 1995.
- [100] P. Phillips, A. Kadi, and O. von Ramm, "Feasibility study for a two-dimensional diagnostic ultrasound velocity mapping system," *Ultrasound in Medicine & Biology*, vol. 21, pp. 217–229, 1995.
- [101] J. Jensen and P. Munk, "A new method for estimation of velocity vectors," *IEEE Trans. Ultrason., Ferroelect., Freq. Contr.*, vol. 45, pp. 837–851, 1998.
- [102] M. Anderson, "Multi-dimensional velocity estimation with ultrasound using spatial quadrature," *IEEE Trans. Ultrason., Ferroelec., Freq. Contr.*, vol. 45, pp. 852–861, 1998.
- [103] M. Anderson, "Vector flow estimator isomorphism and wall filter requirements," *Medical Imaging 2001: Ultrasonic Imaging and Signal Processing*, vol. 4325, pp. 215–226, 2001.
- [104] J. Griffith, W. Brody, and L. Goodman, "Resolution performance of doppler ultrasound flowmeters," *The Journal of the Acoustical Society of America*, vol. 60, pp. 607–610, 1976.
- [105] V. Newhouse, P. Bendick, and L. Varner, "Analysis of transit time effects on doppler flow measurement," *IEEE Trans. Biomed. Eng.*, vol. 23, pp. 381–386, 1976.
- [106] Y. Kim and S. Park, "Modeling of doppler signal considering sample volume and field distribution," *Ultrason. Imaging*, vol. 11, pp. 175–196, 1989.
- [107] A. McArdle and V. Newhouse, "Doppler bandwidth dependence on beam to flow angle," *The Journal of the Acoustical Society of America*, vol. 99, pp. 1767–1778, 1996.

- [108] A. Yu, A. Steinman, and R. Cobbold, "Transit-time broadening in pulsed doppler ultrasound: a generalized amplitude modulation model," *Ultrasonics, Ferroelectrics and Frequency Control, IEEE Transactions on*, vol. 53, pp. 530–541, 2006.
- [109] V. Newhouse, D. Censor, T. Vontz, J. Cisneros, and B. Goldberg, "Ultrasound doppler probing of flows transverse with respect to beam axis," *IEEE Trans. Biomed. Eng.*, vol. 34, pp. 779–789, 1987.
- [110] P. Tortoli, G. Guidi, L. Mantovani, and V. Newhouse, "Velocity magnitude estimation with linear arrays using doppler bandwidth," *Ultrasonics*, vol. 39, pp. 157–161, 2001.
- [111] K.-W. Yeung, "Angle-insensitive flow measurement using doppler bandwidth," *Ultrasonics, Ferroelectrics and Frequency Control, IEEE Transactions on*, vol. 45, pp. 574–580, 1998.
- [112] L. Bohs, B. Geiman, M. Anderson, S. Gebhart, and G. Trahey, "Speckle tracking for multi-dimensional flow estimation," *Ultrasonics*, vol. 38, pp. 369–375, 2000.
- [113] D. Boggs, A. Baktha, J. Hawkins, D. Marr, J. Miller, P. Roussel, R. Singhai, B. Toll, and K. Venkatraman, "The microarchitecture of the intel pentium 4 processor on 90nm technology," *Intel technology journal*, vol. 8, pp. 1–17, 2004.
- [114] G. Trahey, J. Allison, and O. von Ramm, "Angle independent ultrasonic detection of blood flow," *IEEE Trans. Biomed. Eng.*, vol. 34, pp. 965–967, 1987.
- [115] L. Bohs and G. Trahey, "A novel method for angle independent ultrasonic imaging of blood flow and tissue motion," *IEEE Trans. Biomed. Eng.*, vol. 38, pp. 280–286, 1991.
- [116] L. Bohs, B. Friemel, B. McDermott, and G. Trahey, "A real time system for quantifying and displaying two-dimensional velocities using ultrasound," *Ultrasound Med. Biol.*, vol. 19, pp. 751–761, 1993.
- [117] L. Bohs, B. Friemel, and G. Trahey, "Experimental velocity profiles and volumetric flow via two-dimensional speckle tracking," *Ultrasound Med. Biol.*, vol. 21, pp. 885–898, 1995.
- [118] L. Bohs, B. Friemel, J. Kisslo, D. Harfe, K. Nightingale, and G. Trahey, "Three-dimensional flow images by reconstruction from two-dimensional vector velocity maps," *J. Am. Soc. Echocardiogr.*, vol. 8, pp. 915–923, 1995.
- [119] B. Friemel, L. Bohs, K. Nightingale, and G. Trahey, "Speckle decorrelation due to two-dimensional flow gradients," *Ultrasonics, Ferroelectrics and Frequency Control, IEEE Transactions on*, vol. 45, pp. 317–327, 1998.
- [120] L. Bohs, S. Gebhart, M. Anderson, B. Geiman, and G. Trahey, "2-d motion estimation using two parallel receive beams," *IEEE Trans. Ultrason., Ferroelect., Freq. Contr.*, vol. 48, pp. 392–408, 2001.

- [121] L. Bohs, B. Geiman, M. Anderson, S. Breit, and G. Trahey, “Ensemble tracking for 2d vector velocity measurement: Experimental and initial clinical results,” *Ultrasonics, Ferroelectrics and Frequency Control, IEEE Transactions on*, vol. 45, pp. 912–924, 1998.
- [122] S. Bjærum, *Detection and visualization of moving targets in medical ultrasound imaging, paper H: Blood Motion Imaging: A new blood flow imaging technique*. NTNU, 2001.
- [123] D. Goertz, J. Yu, R. Kerbel, P. Burns, and F. Foster, “High-frequency 3-d color-flow imaging of the microcirculation,” *Ultrasound in Medicine & Biology*, vol. 29, pp. 39–51, 2003.
- [124] J. Brown, F. Foster, E. Cherin, and G. Lockwood, “A 40 mhz linear array based on a 2-2 composite with geometric elevation focussing,” *IEEE Ultrasonics Symposium Proceedings*, 2006.
- [125] W. Aoudi, H. Liebgott, A. Needles, V. Yang, F. Foster, and D. Vray, “Estimation methods for flow imaging with high frequency ultrasound,” *In Press, Ultrasonics*, 2006.